Published in final edited form as:

*J Neuroendocrinol*. 2023 November ; 35(11): e13255. doi:10.1111/jne.13255.

# Phospholipase C-ε defines a PACAP-stimulated pathway for secretion in the chromaffin cell

**Xiaohuan Chen**[1], **Breanna L. Coffman**[1], **Rebecca L. Brindley**[2], **Jason D. Galpin**[3], **Christopher A. Ahern**[3], **Kevin P. M. Currie**[2], **Alan V. Smrcka**[4], **Daniel Axelrod**[5], **Arun Anantharam**[1]

[1]Department of Neurosciences, University of Toledo, Toledo, Ohio, 43606, USA

[2]Department of Biomedical Sciences, Cooper Medical School of Rowan University, Camden, New Jersey, 08103, USA

[3]Department of Molecular Physiology and Biophysics, University of Iowa College of Medicine, Iowa City, Iowa, 52246, USA

[4]Department of Pharmacology, University of Michigan, Ann Arbor, Michigan, 48109, USA

[5]Department of Physics and LSA Biophysics, University of Michigan, Ann Arbor, Michigan, 48109, USA

## Abstract

Adrenomedullary chromaffin cells respond to splanchnic (sympathetic) nerve stimulation by releasing stress hormones into the circulation. The signal for hormone secretion is encoded in the neurotransmitters – especially acetylcholine (ACh) and pituitary adenylate cyclase activating polypeptide (PACAP) – that are released into the splanchnic-chromaffin cell synapse. However, functional differences in the effects of ACh and PACAP on the chromaffin cell secretory response are not well defined. Here, selective agonists of PACAP receptors or nicotinic and muscarinic acetylcholine receptors were applied to chromaffin cells. The major differences in the effects of these agents were not on exocytosis, per se, but rather on the steps upstream of exocytosis. In almost every respect, the properties of individual fusion events triggered by PACAP and cholinergic agonists were similar. On the other hand, the properties of the $Ca^{2+}$ transients evoked by PACAP differed in several ways from those evoked by muscarinic and nicotinic receptor stimulation. A defining feature of the PACAP-stimulated secretory pathway was its dependence



**Correspondence** Arun Anantharam, Department of Neurosciences, University of Toledo, Toledo, OH 43606, USA. arun.anantharam@utoledo.edu.
Xiaohuan Chen and Breanna L. Coffman these authors contributed equally.

AUTHOR CONTRIBUTIONS

**Xiaohuan Chen:** Data curation; formal analysis; investigation. **Breanna L. Coffman:** Data curation; formal analysis; investigation. **Rebecca L. Brindley:** Data curation; formal analysis; investigation. **Jason D. Galpin:** Resources. **Christopher A. Ahern:** Resources. **Kevin P. M. Currie:** Data curation; formal analysis; investigation. **Alan V. Smrcka:** Conceptualization; investigation; resources. **Daniel Axelrod:** Formal analysis; software; validation. **Arun Anantharam:** Conceptualization; formal analysis; funding acquisition; investigation; project administration; resources; software; writing – original draft.

CONFLICT OF INTEREST STATEMENT

The authors declare no competing financial interest.

on signaling through exchange protein directly activated by cAMP (Epac) and PLCε. However, the absence of PLCε did not disrupt $Ca^{2+}$ transients evoked by cholinergic agonists. Accordingly, inhibition of Epac activity did not disrupt secretion triggered by acetylcholine or specific agonists of muscarinic and nicotinic receptors. Thus, PACAP and acetylcholine stimulate chromaffin cell secretion via separate and independent pathways. This feature of stimulus-secretion coupling may be important for sustaining hormone release from the adrenal medulla under conditions associated with the sympathetic stress response.

**Keywords**

acetylcholine; chromaffin; exocytosis; PACAP; secretion

## 1 | INTRODUCTION

The “fight-or-flight” response encapsulates a range of physiological changes designed to prepare an individual to respond to a stressor.[1,2] In the periphery, a key effector of the sympathetic nervous system and the flight-or-flight response is the adrenal medulla.[3]

Secretion of catecholamines, peptides, and bioactive molecules from the medulla is dependent on input from preganglionic, sympathetic fibers which pass into the gland via the splanchnic nerves.[4,5] The finding that acetylcholine (ACh) – released from splanchnic nerves onto chromaffin cells in the adrenal gland – causes the subsequent release of catecholamines, was first made by Feldberg and colleagues.[6] We now appreciate that splanchnic neurons also house a variety of peptide neurotransmitters which may be coreleased with ACh to regulate chromaffin cell secretion.[7] Recent evidence suggests that, of these peptides, PACAP may have the most important role.[8-11]

Chromaffin cells express multiple types of nicotinic and muscarinic receptors, in addition to receptors for synaptically-released PACAP. Messenger RNAs for multiple α and β subunits of nicotinic receptors have been identified in the medulla of several model species, with the α3β4 receptor being the predominant form.[12] The nicotinic receptor conducts $Na^+$, $K^+$, and $Ca^{2+}$, although the permeability to $Ca^{2+}$ is probably quite low.[13] ACh-triggered membrane depolarization activates fast, voltage-gated $Na^+$ ($Na_v$) channels to initiate the action potential.[14] Chromaffin cells also express a variety of plasma membrane $Ca^{2+}$ channels.[14,15] These channels open during the action potential and provide an entry pathway for the $Ca^{2+}$ necessary for exocytosis.

Transcripts for all five subtypes of muscarinic receptors have also been identified in chromaffin cells in various species (M1–M5).[16] In the mouse, secretion is most heavily dependent on M1 receptor expression.[17] Activation of M1 receptors stimulates phospholipase C and mobilizes $Ca^{2+}$ via a pathway involving IP3 and caffeine-sensitive internal stores.[18,19] Muscarinic receptor activation has also been linked to changes in membrane potential, resulting in membrane depolarization and even the firing of action potentials, which causes $Ca^{2+}$ influx through plasma membrane $Ca^{2+}$ channels.[19-21]

The molecular mechanisms by which PACAP acts to stimulate secretion are not as well understood. The identity of at least part of the PACAP signaling pathway is encoded in its name – pituitary adenylate cyclase activating polypeptide. Indeed, there is strong evidence that, in the chromaffin cell, stimulation of the PAC1 receptor leads to activation of adenylate cyclase and production of cAMP, leading to increase in $Ca^{2+}$ and fusion.[9-11,22,23] An important difference between the signaling pathways coupling muscarinic receptors and PAC1 receptors to fusion, is that $Ca^{2+}$ entry, rather than mobilization from internal stores, is thought to underlie the secretory response to PACAP in chromaffin cells.[24]

The goal of this study was to elucidate differences in the actions of cholinergic agonists from those of PACAP in the pathways that lead to fusion. To that end, the specific exocytosis-related responses of "wild-type" and PLCε −/− (or KO) chromaffin cells to bethanechol (a non-selective muscarinic receptor agonist) and dimethylphenylpiperazinium (DMPP; a nicotinic receptor agonist) were compared to PACAP. The "responses" of interest here were those that related to changes in intracellular $Ca^{2+}$ that precede membrane fusion, and fusion itself. $Ca^{2+}$ signals in the subplasmalemmal were monitored using a membrane-targeted Lck-GCaMP5G fusion protein.[22,25]

The data show PACAP-stimulated elevations in intracellular $Ca^{2+}$, which increased and decreased with a variable time course, had some resemblance to those evoked by bethanechol. The similarity of the $Ca^{2+}$ responses to stimulation by these agonists likely reflects their common reliance on intracellular signaling pathways coupled to GPCR-activation. The responses to DMPP, on the other hand, had a vastly different form and time course. In most cases, DMPP caused a rapid increase in intracellular $Ca^{2+}$ that decayed slowly over time. Membrane fusion was monitored in TIRF, by measuring release duration of a false fluorescent neurotransmitter (FFN511) packaged in vesicles, or by carbon fiber amperometry.[26,27] Although PACAP and DMPP were more effective secretagogues than bethanechol, the biophysical properties of exocytosis in all other respects, were similar. Importantly, only the effects of PACAP stimulation on intracellular $Ca^{2+}$ and fusion were disrupted by the absence of PLCε. Thus, PACAP and acetylcholine stimulate chromaffin cell secretion via separate and independent pathways. This feature of stimulus-secretion coupling, in which secretory pathways are operationally segregated, is likely to be important for the function of the adrenal medulla, *in situ*.

## 2 | MATERIALS AND METHODS

### 2.1 | Animals

C57BL/6J ("wild-type" or WT) mice were obtained from Jackson Laboratories, Bar Harbor, ME. HA-PLCε and PLCε −/− (also referred to as "KO") mice were generated by Smrcka and colleagues.[28,29] Animals were group housed with 2–5 per ventilated cage with a 12-h dark/12-h light cycle with full access to food and water. Animal proce-dures and experiments were conducted in accordance with the respective University of Toledo (400138) and Rowan University (2017-039) IACUC protocols.

### 2.2 | Mouse chromaffin cell preparation and transfection

Mouse chromaffin cells were isolated and cultured as described previously.[22] Briefly, 2–4-month-old male or female mice were gas anesthetized using an isoflurane beaker technique and sacrificed by cervical dislocation. A total of 2–4 adrenal glands were used for one 35 mm glass bottom dish (14 mm glass diameter; MatTek, cat no. P35G-1.5-14-C) to ensure proper cell density and health of chromaffin cells. Adrenal glands were extracted and moved to dishes containing ice-cold mouse buffer (148 mM NaCl, 2.57 mM KCl, 2.2 mM $K_2HPO_4$•$3H_2O$, 6.5 mM $KH_2PO_4$, 10 mM glucose, 5 mM HEPES free acid, 14.2 mM mannitol). The cortex was carefully removed, and the medullae were rinsed three times in 100 μl drops of papain enzyme solution (450 units/mL Papain; Worthington Biochemical, cat no. LS003126), 250 μg/ml bovine serum albumin (BSA; Sigma-Aldrich, cat no. A7906), and 75 μg/ml dithiothreitol (Roche, cat no. 10708984001) in mouse buffer). The medullae were then transferred to a 15-ml falcon tube containing 0.5 ml of papain solution and placed in a water bath shaker for 15 min at 37°C shaking at 140 rpm. After 15 min, the digesting solution was mostly removed and replaced by 0.5 ml of collagenase enzyme solution (250 μg/ml BSA, 0.375% collagenase (Sigma-Aldrich, cat no. C0130), and 0.15 mg/ml DNase I (Sigma-Aldrich, cat no. DN25) in mouse buffer). Digestion was continued for another 15 min at 37°C shaking at 140 rpm. The digested medullae were then transferred to antibiotic-free culture medium (Dulbecco's Modified Eagle's Medium/F12 (DMEM/F12; ThermoFisher Scientific, cat no. 11330-032) supplemented with 10% fetal bovine serum (FBS) (ThermoFisher Scientific, cat no. 11403-028). The medullae were then triturated by push-pull movement using a 1000 μl pipette tip. The suspension was then centrifuged at 1300× *g* for 2.5 min. The supernatant was discarded and the pellet was resuspended in 300 μl of antibiotic-free medium supplemented with 10% FBS. If transfection was desired, the pellet was instead resuspended in 110 μl of R buffer (Invitrogen, cat no. MPK10096). The desired plasmid was added to the mixture (1.25 μg/gland). The suspended cells were transiently transfected by electroporation with a single pulse (1050 mV, 40 ms) using the neon transfection system (Invitrogen, cat no. MPK5000 and cat no. MPK10096). Before the start of the cell preparation, MatTek 35 mm glass bottom dishes were precoated with Matrigel (Corning, cat no. 356230) diluted in DMEM/F12 (1:7) for 1–1.5 h after which the dishes were washed with DMEM/F12. After electroporation, 200 μl of antibiotic-free medium was added to the cells and all the mixed cell suspension was deposited in the coated dish (at least 2 dishes per condition). The cells were cultured in an incubator (37°C, 5% $CO_2$) for approximately 4 h. A culture medium with antibiotics was then added to a final volume of 2 ml (DMEM/F12 supplemented with 10% FBS, 9.52 unit/ml penicillin, 9.52 μg/ml streptomycin, and 238 μg/ml gentamicin (ThermoFisher Scientific, cat no. 15140-122 and cat no. 15710-064)). The media was replaced the day after plating and experiments were conducted between 24 and 48 h after plating.

The Lck-GCaMP5G plasmid was obtained from Addgene (cat no. 34924). The PLCε-FLAG-P2A-mCherry plasmid was synthesized and cloned into a pCMV-script EX vector by GenScript company. For rescue experiments in the PLCε KO chromaffin cells in which the PLCε-FLAG was overexpressed, transfected cells were identified based on their mCherry fluorescence.

### 2.3 | TIRF microscopy

A two-line (488 nm/561 nm) Olympus cellTIRF microscope system (Olympus) was used to perform TIRF imaging. The microscope utilizes TIRF oil-immersion objectives (NA 1.49, 60×, and 100×) with an additional 2× lens in the emission path between the microscope and the camera (Andor Technology, iXon 897). The final pixel size of the images was 80 nm.

All TIRF experiments were performed between 35 and 37°C by placing the dish on the temperature controller platform (Warner instruments, cat no. TC-324C). Physiological salt solution (PSS) buffer was prepared (145 mM NaCl, 5.6 mM KCl, 2.2 mM $CaCl_2$, 0.5 mM $MgCl_2$, 5.6 mM glucose, and 15 mM HEPES, pH 7.4) and prewarmed to 37°C before experiments were performed. The culture medium was replaced with PSS before the experiment and changed after each stimulation. Chromaffin cells were individually stimulated using a needle (100-μm inner diameter, ALA Scientific Instruments, cat no. ALA QTP) connected to a positive-pressure perfusion system (ALA Scientific Instruments, ALA-VM4). Acetylcholine was purchased from Sigma (cat no. A6625). For experiments in which 1,1-Dimethyl-4-phenylpiperazinium iodide (DMPP; Sigma-Aldrich, cat no. D5891), bethanechol (TCI Chemicals, Cat# B4828), and pituitary adenylate cyclase-activating polypeptide 1–38 (PACAP; Tocris, cat no. 1186; or synthesized at University of Iowa by J. Galpin and C. Ahern [see below]) were applied sequentially, cells were exposed to PSS for 5 s and then stimulated either with 1 μM PACAP or 100 nM bethanechol for 60 s first, washed with PSS for 30 s and then stimulated with 1 μM DMPP for 60 s. Where indicated, cells were incubated with 100 μM FFN511 (Abcam, cat no. ab120331) in PSS buffer for 30 min at 37°C and washed with PSS prior to imaging on the TIRF microscope. ESI-09 (Tocris, cat no. 4773) was added to the bath to a final concentration of 1 μM for at least 10 min prior to stimulation with agonist. Where used, 10 μM 8-(4-Chlorophenylthio)-2‰-*O*-methyladenosine-3′, 5′-cyclic monophosphate acetoxymethyl ester (cpTOME-AM; Tocris, cat no. 4853) was applied directly to cells via a perfusion pipet while secretion was monitored in TIRF.

### 2.4 | Synthesis of PACAP peptide HSDGI FTDSY SRYRK QMAVK KYLAA VLGKR YKQRV KNK

The peptide PACAP 1–38 was synthesized on a Liberty Blue peptide synthesizer (CEM Corp.) as a C-terminal amide at 0.025 mM scale using standard Fmoc synthetic methods and piperidine deprotection. The peptide was cleaved from resin and deprotected using a trifluoroacetic acid cocktail at 37°C for 30 min and precipitated using ice-cold diethyl ether. The crude peptide was purified on a Waters 1525 HPLC and Sunfire semi-prep C18 column, fitted with a 2998 photodiode array detector, using a linear gradient of water/acetonitrile, each containing 0.2% trifluoroacetic acid. Fractions containing the peptide were combined and lyophilized overnight. The fluffy white residue was analyzed by a Waters QToF Premier spectrometer in positive ion mode. Strong peaks for M +3, +4, +5 … +8 were observed, for a deconvoluted mass of 4515 Da (calculated mass 4534 Da), indicating a loss of water in the spectrometer. The HPLC trace at 220 nm absorbance indicates two peaks at 10.9 and 14.6 min which may indicate the folded and unfolded forms of the peptide.

### 2.5 | Immunohistochemistry and immunocytochemistry

Two to four month old HA-PLCε transgenic mice (male and female) were gas anesthetized using an isoflurane beaker technique and sacrificed by cervical dislocation. The mice were immediately exposed to cardiac perfusion using 30 ml of ice-cold PBS (ThermoFisher, cat no. 10010-023) followed by 10 ml of 4% paraformaldehyde (PFA) (Electron Microscopy Sciences, cat no. 19208). Adrenal glands were removed. Fat and connective tissues surrounding the glands were trimmed off. Glands were then kept in 5 ml of 4% PFA for 2 h and then immersed in a series of sucrose solutions (10%, 15%, and 30% in PBS) until they sink to the bottom of the conical tube. After that, they were individually transferred to a mold containing optimal cutting temperature (O.C.T) media (Fisher HealthCare, cat no. 23-730-571) and snap-frozen using dry ice. Slices were then obtained using a cryostat with a section thickness of 8 μm. Upon staining, slices were fixed with 4% PFA for 10 min and washed 3× with PBS at room temperature. Following fixation, slices were permeabilized using 0.2% Triton X-100 (Sigma-Aldrich, cat no. T8787) in PBS for 15 min. Slices were then blocked with 20% horse serum (ThermoFisher Scientific, cat no. 26050088) in PBS for 1 h at room temperature. After blocking, slices were incubated with recombinant rabbit monoclonal HA antibody (Thermo Fisher Scientific, cat no. MA5-27915, RRID:AB 2,744,968, clone RM305, dilution 1:500) and mouse monoclonal KDEL antibody (Enzo Life Sciences, cat no. ADI-SPA-827, RRID:AB_10618036, clone 10C3, dilution 1:200) at 4°C overnight. On the following day, slices were washed 3× for 15 min each with PBST (PBS+ 0.1% Tween-20, Fisher bioreagents, cat no. BP337) with gentle shaking and incubated with secondary antibodies diluted in blocking buffer for 1 h at room temperature. Fluorescently conjugated secondary antibodies, Alexa Fluor 488-donkey anti-rabbit IgG (H + L) (Thermo Fisher Scientific, cat no.A-21206, RRID:AB_2535792, dilution 1:500) and Alexa Fluor 568-donkey anti-mouse IgG (H + L) (Thermo Fisher Scientific, cat no. A10037, RRID:AB_2534013, dilution 1:500) were used. Secondary antibodies were washed three times with PBST for 15 min each and mounted with DAPI Fluoromount G (SouthernBiotech, cat no. 0100-20).

For immunocytochemistry, freshly dissociated chromaffin cells were cultured in 35 mm MatTek glass bottom dishes for 24–48 h after which the culture medium was removed. Cells were then washed 3× with PBS. Cells were fixed with 4% PFA for 10 min and washed 3× with PBS. Following fixation, cells were quenched with 50 mM $NH_4Cl$ for 15 min and washed with PBS for 5 min. After that, cells were permeabilized using 0.2% Triton X-100 in PBS for 10 min and blocked with 20% horse serum in PBS for 1 h at room temperature. Cells were incubated with rabbit polyclonal anti-PLCE1 antibody (Thermo Fisher Scientific, cat no. PA5-100856, RRID:AB_2850354, dilution 1:100) at 4°C overnight. The following day, cells were washed 3x for 15 min each with PBST and incubated with Alexa 594 conjugated donkey anti-rabbit IgG (H + L) antibody (Thermo Fisher Scientific, cat no. A-21207, RRID:AB_141637, dilution 1:500) for 1 h at room temperature. Cells were washed 3× with PBST for 15 min each and mounted with DAPI Fluoromount G.

All confocal images were taken using the Leica TCS SP5 multiphoton laser scanning confocal microscope, equipped with a 63× oil immersion objective. An additional zoom-in strength of 3x was applied to the field of interest using the microscope's software. All

images were taken in a sequential scan mode according to the laser channels. Excitation was accomplished using 405-, 488-, 568, and 594-nm lasers. All images were further processed using ImageJ Fiji software.

### 2.6 | Colocalization analysis

The JACoP plugin on ImageJ was used to obtain Manders coefficients of green (Alexa 488) and red (Alexa 568) areas of interest which correspond to antibody-labeled PLCε-HA and KDEL proteins, respectively. Because PLCε is only expressed in adrenomedullary chromaffin cells, and not in cells of the adrenal cortex, the Manders coefficient analysis was only performed on regions of interest from the adrenal medulla. Each selected cell was then exposed to a thresholding setting using the JACoP ImageJ plugin, described in detail by Bolte et al. (2006).[30] The M1 and M2 coefficients were automatically calculated by the plugin.

### 2.7 | Image analysis of FFN511 fusion events

Fusion events were visually identified. Regions of interest (ROIs) of 480 nm were then selected using the Time Series Analyzer version 3.0 plugin on Fiji software. A nearby ROI, where no fluorescent punctum was evident, was used for background subtraction. Images were acquired at approximately 48 Hz. The duration of FFN511 release was measured with a program custom-written in Interactive Data Language (IDL; ITT, Broomfield, CO). Details of how the program works are described elsewhere.[22]

### 2.8 | Analysis of $Ca^{2+}$ responses

The fluorescence intensity versus time ($F$ vs. $t$) response to agonists is usually irregular in shape, varying both between different agonists and run-to-run on different cells with the same agonist. The variability is due to: (a) photon shot noise (along with camera readout noise and dark noise), which adds noise equally at all frequencies (i.e., white noise); (b) a slowly varying background, probably due to optical scattering from outside the observation zone, cell motion; (c) variable release and dissipation rates of fluorophore from multiple releases within the region of interest (ROI); and (d) cell biological variability. To characterize the diverse responses in a manner in which a robust comparison of different agonists can be made, several features of the $F$ versus $t$ curves are analyzed. These features are not completely independent, but neither are they identical, and together they combine to make different agonist responses quite distinct.

**2.8.1 | Spike times and widths—**The response is a composite of individual “spikes”, which partially superimpose to produce maxima in $F$ versus $t$. To measure the height of each, we smooth out the shot noise, and then find an appropriate local “baseline” on the basis of which heights and widths can be measured. With a program custom written in IDL the smoothing is accomplished by convolution with a Gaussian shape of user-input width. The width should be as wide as possible to overcome shot noise, but not so wide as to distort the overall shape of the $F$ versus $t$ response. We chose a half-width of 200 time-bins (10 s) at the $e^{-2}$ height of the convolving Gaussian; it produces a smoothed response curve that follows the original data well (Figure 1A). Next, the time locations of all the extrema (maxima and minima) are identified in the smoothed response. For each maximum (shown

in green), the two surrounding minima are identified, and a straight line connecting the two minima is drawn, the “local baseline” (shown as a black dashed line). The fluorescence intensity “height” $h$ of the surrounded maximum is then defined as the $F$ ordinate distance from the smoothed maximum vertically down to the local baseline.

Many of the maxima are very small and indistinguishable from possible noise. Therefore, we impose a criterion for accepting a maximum: it must have a height $h$ that is at least half as big as its local baseline height $b$. Of those maxima that pass this acceptance test, the time duration of the maximum is defined as its full width at height $h / 4$ as measured up from its local baseline (blue double arrow). The “average duration” is simply the mean of the durations of all the acceptable maxima. The “%ΔF/F Max” is the maximum amplitude of the record above the local baseline.

**2.8.2 | Autocorrelation—**The responses to some agonists appear qualitatively more “jittery” than do others: their fluctuations appear more rapid. To quantitatively characterize the overall rapidity of fluctuations, we generate the autocorrelation function $G(\tau)$ of the fluorescence versus time. In its full mathematical generality,

$$G(\tau) \equiv \int_0^\infty \Delta F(t)\Delta F(t+\tau)dt \quad \text{(Equation 1)}$$

where $\Delta F(t) \equiv F(t) - \langle F \rangle$ and $\langle F \rangle$ is the mean of $F(t)$ over all time. $G(\tau)$ reports how rapidly the deviation of a function from its mean, $\Delta F(t)$, “forgets” what its value had been at time $\tau$ earlier. For example, $G(0)$ is just the integral of $(\Delta F)^2$, an integrand which is always positive. But as $\tau$ becomes larger, some of the integrand products become negative and the integral becomes smaller. The more rapid the fluctuations (on average), the more rapidly $G(\tau)$ decays with $\tau$.

If the fluctuations were composed of superimposed individual spikes, and these spikes occurred at random times, then the autocorrelation function of the whole trace would have the same shape as the autocorrelation function of an individual spike. However, since we do not know how the occurrence of individual spikes might be time-correlated with each other, the overall shape of the autocorrelation function cannot be so overinterpreted. However, its initial slope can be useful, as discussed below.

The autocorrelation function is mathematically related to another measure of fluctuation rapidity, the Fourier transform. However, use of $G(\tau)$ has a big advantage in this application. Much of the fluctuation is instrumental in origin: shot noise, and camera readout and dark noise. These sources produce an intrinsically random number of observed photons around a mean, even at constant light intensity. A fluctuation in the signal above the mean does not predict at all whether the next time bin will be above the mean or below the mean. Instrumental noise has essentially zero memory. Therefore, its contribution to $G(\tau)$ is entirely confined to the $\tau = 0$ channel. On the other hand, the negative initial slope of $G(\tau)$ as $\tau$

increases from 0+ is proportional to the rapidity of fluctuations in $\Delta F(t)$ that is intrinsic to its underlying intensity and is not biased by instrumental noise.

Actual computer calculations of $G(\tau)$ cannot use Equation 1 directly because the duration of the signal is finite, not infinite, and because the time scale is broken into uniform (but small) discrete time bins. For finite-sized and discrete time bins, Equation 1 can be rewritten:

$$G(L) = \frac{1}{N} \sum_{k=0}^{N-L-1} (F_k - \langle F \rangle)(F_{k+L} - \langle F \rangle)$$

(Equation 2)

where $L$ is an integer number of "time lag" bins analogous to the continuous $\tau$ time delay argument. In these studies, $N$ is usually in the thousands. We are interested only in the time behavior of G(L). We do not want it affected by the absolute size of $F_k$. Therefore, $F_k$ is understood to be the pre-normalized fluorescence (normalized to the mean) and so the normalized $\langle F \rangle = 1$.

To avoid the shot noise peak at $L = 0$, an extrapolation of $G$ toward $L = 0+$, called $G_{\text{fit}}(0+)$ here, can be obtained by least-squares fitting the first few (here, 10) non-zero L points (i.e., $L = 1, 2, \ldots 10$) in $G$ to a second-degree polynomial (i.e., a parabola) and evaluating the parabola's value at $(L = 0)$. Also, the initial slope $G'_{\text{fit}}( = dG_{\text{fit}} / \text{dL})$ can be calculated directly from that fitted parabola by taking its derivative and evaluating it at $L = 0$. This procedure is illustrated in Figures 1B,C.

Since the original data is of finite duration, $G(L)$ at larger $L$ is not reliable: the calculation for $G$ does not see enough slow fluctuations to get a good estimate of their average behavior. However, the downward initial (i.e., small $L$) slope of the green line fit is based on far more fluctuations and is a reliable measure of average fluctuation rapidity.

The initial slope as reported here must be appropriately normalized so it is a function only of the average rapidity of $\Delta F(t)$ and not of absolute $\Delta F(t)$ size. We hereby report the following normalized initial slope, with the variables identified on Figure 1B.

$$g'_{\text{fit}}(0) = -\frac{G'_{\text{fit}}(0)}{G_{\text{fit}}(0)}$$

(Equation 3)

## 2.9 | Carbon fiber amperometry

Amperometry data was collected using 5 μm diameter carbon fiber electrodes (CFE-2; ALA Scientific Instruments) (for detailed description see[31]). A potential of +700 mV was applied to the electrode and data recorded using a VA-10X amplifier (NPI Electronic, GmbH), connected to a 16-bit BNC-2090 analog to digital converter (National Instruments), and WinEDR software written by Dr John Dempster (Strathclyde University, Glasgow, Scotland). Data were filtered at 2 kHz and sampled at 10 kHz. The carbon fiber electrodes

were used multiple times and carefully cut back between every cell to reveal a fresh oxidation surface and to minimize electrode fouling. The recording bath (volume ~300 μl) was continuously perfused with fresh extracellular solution from gravity fed reservoirs at a rate of ~3 ml/min. The extracellular recording solution contained (in mM): 145 NaCl, 2 KCl, 1 MgCl2.6H2O, 10 glucose, 10 HEPES, 2 CaCl2, pH 7.3 and osmolarity ~305 mOsm. Secretion was stimulated either by bath application of carbachol (100–300 μM, a non-selective cholinergic agonist), DMPP (10 μM), or PACAP (100 nM). Amperometric spikes were detected and analyzed using the Quanta Analysis macros written by Dr. Eugene Mosharov[32] in IgorPro software (Wavemetrics Inc.) as previously described.[31] Detection criteria were: amplitude ≥3pA; rise time <10 ms; foot amplitude >1pA; foot duration >1 ms. To count the number of spikes evoked by each agonist all spikes meeting these criteria were included unless they overlapped by >50% (determined in the analysis macro). To calculate individual spike and foot parameters, only non-overlapping spikes were included (defined as <10% overlap in the spike detection software). All detected spikes were confirmed by visual inspection.

### 2.10 | Statistical analysis for amperometry

For statistical comparisons in amperometry experiments the median values for each spike parameter (as detailed in results section) were calculated for each cell and these cell averages were pooled for statistical comparison using the Kruskal-Wallis test followed by Dunn's test for multiple pairwise comparisons. This approach means that each cell has the same statistical weight in the analysis (for further discussion see[32,33]). The number of spikes was compared using one-way ANOVA with Tukey's test for multiple pairwise comparisons.

### 2.11 | Statistical analysis for imaging

GraphPad Prism was used for all statistical analysis. Curve fitting was performed on Origin 2020b or IDL as described in the Methods. The distribution of values for a particular data set were first assessed for normality with a Shapiro–Wilk test. Differences in means of normally distributed data were subsequently compared using a *t*-test with Welch's correction. A Mann–Whitney test was used to compare data sets whose individual values were not normally distributed.[34] For multiple comparisons, either a One-way ANOVA (normally distributed data) with Tukey's test or Kruskal-Wallis with Dunn's test was used to compare data sets. Values reported are means ± standard deviations (SD) for normally distributed data, or medians with 25th and 75th percentile values for non-normally distributed data. Exact *p*-values are reported, except in the case where $p > .99$. Within figures, the symbol ns means $p > .05$, * means $p \leq .05$, ** means $p \leq .01$, *** means $p \leq .001$, and **** means $p \leq .0001$. In a few cases within the study, the number of asterisks might not match the scheme described here. This is because the *p*-value was obtained by rounding up or rounding down. *p*-values are reported to 1 significant digit. All other values are reported to 2 or 3 significant digits.

# 3 | RESULTS

## 3.1 | Chromaffin cell $Ca^{2+}$ responses to PACAP, DMPP, and bethanechol

PACAP and acetylcholine represent two of the most important secretagogues in the adrenal medulla. To differentiate the effects of these agents on the fusion pathway within chromaffin cells, we first characterized the $Ca^{2+}$ signals evoked by PACAP stimulation (Figure 2B). Then, we quantified the differences between these signals and others caused by cholinergic agonists. In all cases, changes in intracellular $Ca^{2+}$ were studied using the genetically-encoded $Ca^{2+}$ indicator, GCaMP5G, fused to the N-terminal domain of Lck.[25,35] Lck causes membrane targeting of GCaMP5G, greatly improving the signal within the region of the cell best imaged by TIRF (Figure 2A).

PACAP caused a complex pattern of $Ca^{2+}$ transients, an example of which is presented in Figure 2A. In some cases, as in the example provided in Figure 2B, $Ca^{2+}$ levels fluctuated rapidly, peaking then collapsing to a short-lived plateau, or back to baseline. In other cases, transients climbed to a long-lived plateau of a variable amplitude. The heterogeneous pattern of $Ca^{2+}$ responses to PACAP were more remarkable when juxtaposed with those caused by the selective nicotinic agonist, DMPP. While PACAP caused $Ca^{2+}$ responses that, as a rule, varied, DMPP usually caused a large and slowly desensitizing $Ca^{2+}$ transient (Figure 2D). A third agonist, bethanechol, produced changes that were visually similar to those caused by PACAP. As the example in Figure 2E shows, bethanechol caused elevations in intracellular $Ca^{2+}$ that exhibited a variable time course and amplitude. The smoothed records, convolved with a Gaussian of a defined width (used for maxima detection), are shown in Figure 2C, or in the inset of Figures 2D,E. The location of automatically identified maxima are indicated by the green solid lines.

Important features of the fluorescence intensity (%ΔF/F) versus time records were extracted and presented in Figures 3A,E. The maximum amplitude of the $Ca^{2+}$ transient evoked by DMPP, bethanechol, or PACAP was identified, and registered on the graph in Figure 3A as an open square, circle, or triangle, respectively. On average, the peak amplitude of the response to DMPP and PACAP was significantly greater than it was to bethanechol. The average duration of the individual agonist-evoked $Ca^{2+}$ maxima within a record was shorter when PACAP or bethanechol was applied to cells, than DMPP (Figure 3B). The average number of maxima within a record was greater for PACAP and bethanechol than for DMPP, reflecting the variable nature of the $Ca^{2+}$ responses in cells stimulated by these agonists (Figure 3C). Finally, the pattern of the $Ca^{2+}$ response to the agonists was captured in quantitative terms. Some of the fluorescence records were clearly more “jittery” or exhibited more fluctuations than others. This jitteriness was described using the initial slope of the autocorrelation function (see Methods). On average, the values resulting from this calculation were significantly greater for PACAP and bethanechol, than they were for DMPP (Figure 3D). This validates, in quantitative terms, the observation that the fluorescent responses to PACAP and bethanechol were more heterogenous with more rapid fluctuations than the responses to DMPP.

### 3.2 | Effects of PACAP compared to cholinergic agonists on secretion

Next, the secretory responses of chromaffin cells to stimulation by either PACAP, or the cholinergic agonists, was monitored with TIRF microscopy. For these studies, chromaffin cells were briefly incubated with the fluorescent compound FFN511 to label secretory vesicles.[22,26] Cells were subsequently stimulated by DMPP, bethanechol, or PACAP for 60 s. Two examples of exocytotic events in which FFN511-labeled vesicles fused and released their fluorescent cargos, are shown in Figure 4A. The corresponding fluorescence intensity versus time curves for the events can be found to the right of the image series. Overall, no difference in the release duration of FFN511 was observed in cells exposed to either of the three agonists used in these studies (Figure 4B). Differences in the number of fusion events stimulated by DMPP, bethanechol, and PACAP was also assessed. Because more fusion events might be expected to occur in a larger cell, the number of fusion events was normalized to the surface area of the cell footprint and reported as events per square micron (Figures 4C,D). DMPP and PACAP caused significantly more fusion events per unit area than bethanechol.

While TIRF microscopy has excellent spatial resolution, it lacks the time resolution of some other non-optical methods. A method with substantially better time resolution than TIRF – carbon fiber amperometry – was used to validate imaging studies and to obtain additional information, not accessible to TIRF, regarding the characteristics of the early fusion pore. The carbon fiber electrode was positioned immediately adjacent to a chromaffin cell (Figure 5A). Secretion was evoked by perfusing the cell with carbachol (a non-selective cholinergic agonist), DMPP, or PACAP. Each upward “spike” on the current trace reflects oxidation of catecholamines released from a single secretory vesicle fusion event.[27,36,37]

Amperometry showed PACAP and DMPP to cause significantly fewer spikes per cell (i.e., fusion events) than carbachol (Figure 5B, Table 2). The amount and kinetics of transmitter release from individual fusion events was also compared (Figure 5C). For each cell, the median charge, amplitude, duration, and slope of the spikes was calculated. The charge (area) of the spikes is directly proportional to the number of catecholamine molecules released during the vesicular fusion event and was not significantly different in cells stimulated with PACAP compared to either carbachol or DMPP (Figure 5C, Table 2). There was also no significant difference in the amplitude, rising slope, or duration of the spikes at half maximal amplitude (half-width) when comparing PACAP with the cholinergic agonists (Figure 5C, Table 2).

It is well-documented that a prespike “foot” is discernible before the rising phase of some amperometric spikes (Figure 5D), and this is thought to be due to the release of catecholamine through the initial, narrow fusion pore prior to expansion of the pore and more rapid transmitter release seen during the main spike.[36,38,39] The frequency with which a foot was documented, varied as a function of the secretagogue (Table 3). However, there were no statistically significant differences between any of the groups when comparing the spike parameters (charge, amplitude, half-width, slope) (Table 3) or the characteristics of the foot itself (charge, duration, amplitude) (Figure 5D, Table 3).

### 3.3 | Immunolocalization of phospholipase C epsilon (PLCε) in chromaffin cells

We previously reported that PLCε was expressed in chromaffin cells and had a key role in regulating exocytosis stimulated by PACAP. Here, we elaborated on the role of PLCε, by investigating, first, its localization, and then its role in the fusion pathways associated with cholinergic and PACAP stimulation.

Adrenal glands from transgenic hemagglutinin-tagged PLCε (HA-PLCε) were used to investigate the subcellular localization of PLCε.[28] As Figure 6A shows, abundant PLCε expression was detected in the adrenal medulla, but interestingly, not in the adrenal cortex. Much of the PLCε expression within chromaffin cells appeared to be perinuclear (Figures 6A,B). To validate this supposition, adrenal sections were exposed to antibodies not only for HA – to visualize PLCε – but also KDEL (Lys-Asp-Glu-Leu). The KDEL antibody recognizes proteins housed within the endoplasmic reticulum.[40] Colocalization of KDEL and PLCε was evaluated with an ImageJ plugin (see Methods). This analysis showed that anti-HA fluorescence did frequently overlap with anti-KDEL fluorescence, consistent with a distribution to organelles, such as the endoplasmic reticulum, near the nucleus (Figure 6C).

Some of the immunofluorescence associated with anti-HA appeared to originate from plasma membrane of chromaffin cells. However, the process of sectioning made it difficult to preserve the plasma membrane for imaging studies. Therefore, immunostaining for endogenous PLCε in dissociated chromaffin cells was also performed. These experiments showed PLCε frequently had a perinuclear distribution (Figure 6D, arrow), which was similar to its distribution in adrenal sections. In other instances, PLCε-positive fluorescence appeared to ring the outside of the imaged cell, consistent with a plasma membrane localization (Figure 6E, arrows).

### 3.4 | $Ca^{2+}$ signals and fusion in PLCε KO cells

We previously reported that intracellular $Ca^{2+}$ responses to PACAP stimulation were severely disrupted in cells that lacked expression of PLCε.[22] However, a potential role of PLCε in regulating $Ca^{2+}$ responses to either DMPP or bethanechol has not been studied. Therefore, WT and PLCε KO chromaffin cells expressing Lck-GCaMP5G were sequentially stimulated with either PACAP and DMPP, or bethanechol and DMPP (Figure 7). In WT cells, PACAP-evoked $Ca^{2+}$ responses exhibited their characteristic fluctuations. And, consistent with results reported in Figure 2, $Ca^{2+}$ responses to DMPP increased to a peak, and then decayed slowly (Figure 7B). A “wash” interval of 30 s was imposed during the period that preceded DMPP stimulation. However, $Ca^{2+}$ signals consistent with continued PACAP stimulation were frequently observed during this period. This suggests that PACAP was not readily “washed out” prior to application of DMPP, and/or the underlying mechanisms causing $Ca^{2+}$ changes inactivate slowly (Figure 7B). When the amplitudes of the $Ca^{2+}$ responses to DMPP and PACAP were averaged, it was evident that only the responses to PACAP were compromised in the KO (Figure 7F). This paradigm was repeated, with bethanechol replacing PACAP in the initial phase of stimulation. The $Ca^{2+}$ signals elicited by bethanechol resembled those elicited by PACAP; and, similar to PACAP, small fluctuations in fluorescent $Ca^{2+}$ signals were observed during the wash

interval (Figure 7D). However, unlike PACAP, the bethanechol-stimulated ΔF/F signal was not deleteriously affected by the absence of PLCε (Figures 7E,G).

Finally, we compared the secretory responses of WT and PLCε KO cells to PACAP and cholinergic agonists. PACAP-stimulated exocytosis in WT cells was strongly suppressed in cells exposed to 1 μM ESI-09 – a membrane permeable Epac inhibitor (Figure 8A). This result was not unexpected, given the known dependence of PLCε on Epac activity.[41] However, ESI-09 did not inhibit secretion in cells stimulated by bethanechol, DMPP, or acetylcholine. (Figures 8A,B). The secretory responses of WT and PLCε KO chromaffin cells to cpTOME – a cAMP analog that stimulates Epac activity – was also measured (Figure 8C). We previously reported that cpTOME application increases intracellular $Ca^{2+}$ levels in WT chromaffin cells.[22] Data reported in Figure 8C show that the ability of cpTOME to trigger secretion is severely compromised in cells that lack PLCε. Evidently, functional communication between Epac, PLCε, and downstream elements of this signaling pathway are necessary for optimal cpTOME-triggered release. Although rare excytotic events were observed in KO cells stimulated by PACAP, their frequency was not different to WT cells "stimulated" by a basal solution (Figure 8C). Thus, such events are most likely spontaneous (spnts) and not triggered specifically by PACAP application (Figure 8C). To show that the disruption of PACAP-stimulated release in KO cells was due specifically to the absence of endogenous PLCε, release was rescued by overexpression of exogenous PLCε (see PACAP resc. lane in Figure 8C).

## 4 | DISCUSSION

We previously reported that chromaffin cell secretion caused by PACAP, but not acetylcholine, was sensitive to the expression of PLCε.[22] The major implication of that study was that the secretory pathways defined by PACAP and acetylcholine stimulation were independent of one another. However, we did not attempt to differentiate between the roles of nicotinic and muscarinic receptors, whose dependence, or lack of dependence, on PLCε may not be equivalent. In this study, properties of PACAP and selective nicotinic (DMPP) and muscarinic (bethanechol) agonists on the secretory pathway in chromaffin cells were systematically investigated using a combination of TIRF microscopy, amperometry, and novel image analysis routines. The results reported herein substantiate the idea that PACAP and cholinergic agonists regulate secretion through distinct, non-overlapping signaling pathways.

### 4.1 | Pathways coupling receptor activation to increases in $Ca^{2+}$ and fusion

The pattern of $Ca^{2+}$ signals evoked by DMPP (this study) and ACh[22] are similar. This suggests that the major effects of exogenous ACh on chromaffin cells are mediated by nicotinic receptors. On the other hand, the similar appearance of $Ca^{2+}$ signals evoked by bethanechol and PACAP (Figures 2, 7) belie deep differences in the pathways they activate. The M1 receptors, presumed to be most highly expressed in the medulla, couple to $G\alpha_q$ to stimulate PLC activity and produce IP3.[42] The subsequent increase in $Ca^{2+}$ that causes exocytosis is thought to originate from caffeine-sensitive internal stores.[43] We recently showed that PACAP-stimulated release in chromaffin cells requires PLCε. This

requirement suggests its reliance on a $G\alpha_s$-coupled pathway, that signals through cAMP and Epac (Figure 8). Indeed, when Epac activity was inhibited with ESI-09, or when PLCε KO cells were stimulated with cpTOME, little to no secretion was detected (Figure 8). Here, we provide further evidence that the pathways coupling muscarinic receptors and PAC1 receptors to secretion must be regulated through different effectors. While the $Ca^{2+}$ response to PACAP was severely disrupted in PLCε KO cells, no appreciable effect on the bethanechol-stimulated $Ca^{2+}$ response was observed (Figure 7). Operational independence of the nicotinic/muscarinic-stimulated pathways and PACAP-stimulated pathways for secretion is also demonstrated by Figures 8B,C. These data show that neither the secretory responses to DMPP nor ACh depend on signaling through Epac and PLCε.

On average, the fluorescent $Ca^{2+}$ signals stimulated by bethanechol were of a smaller amplitude than those stimulated by PACAP or DMPP (Figure 3A). Notably, the amplitude of the $Ca^{2+}$ signal bethanechol stimulates was not increased by raising its concentration from 100 nM to 1 μM (Average %ΔF/F Max ± SEM for 1 mM bethanechol = 61 ± 15; 100 nM bethanechol = 72 ± 12). On the other hand, the maximum amplitude of the PACAP-evoked ΔF/F was similar to the DMPP-evoked ΔF/F. One can speculate that at least part of the reason for the difference in amplitudes between bethanechol versus PACAP/DMPP, is that both PACAP and DMPP pathways draw from a deeper reservoir of $Ca^{2+}$ (the external medium) than bethanechol, with also more pathways for entry into the cytosol.

We recently reported that a brief exposure of chromaffin cells to PACAP causes a long-lasting increase in cytosolic $Ca^{2+}$ that at least partially depends on $Ca^{2+}$ influx through voltage-gated channels.[22] However, the pattern of the $Ca^{2+}$ change caused by PACAP, its fluctuations and variable time course, do suggest that an additional $Ca^{2+}$ source might be involved. In cardiac myocytes, $Ca^{2+}$-induced $Ca^{2+}$ release (CICR) is an important contributor to the overall $Ca^{2+}$ signal.[41] A similar pathway could be important in chromaffin cells.

Signaling through PLCε may gate $Ca^{2+}$ release from internal stores. A potential role for PLCε in such a pathway is supported by previous studies,[44] and immunolabeling experiments (Figure 6). Based on the fluorescent profile of PLCε immunolabeling, much, if not most, of the protein is localized to perinuclear regions of the cell, including, possibly, the Golgi and the endoplasmic reticulum. In the chromaffin cell, the endoplasmic reticulum is a rich storage depot for $Ca^{2+}$.[15] The localization of PLCε to the endoplasmic reticulum, might provide opportunities for spatially localized (i.e., compartmentalized) signaling, allowing for efficient and rapid release of $Ca^{2+}$ into the cytosol.[45]

The genetically-encoded $Ca^{2+}$ indicator employed here is most useful for monitoring qualitative rather than quantitative changes in $Ca^{2+}$. However, it is probably true that PACAP and DMPP cause greater increases in $[Ca^{2+}]_i$ than does bethanechol. Accordingly, the fusion "density" of cells – reported as events/$\mu m^2$ – stimulated by bethanechol is lower than it is in cells stimulated by PACAP or DMPP (Figure 4). The number of fusion events (i.e., spikes) in cells stimulated by carbachol and detected by amperometry, however, was higher than it was in cells stimulated by either PACAP or DMPP (Figure 5). $Ca^{2+}$ imaging studies with carbachol were not performed. We presume the greater number of fusion events evoked

by carbachol is directly related to a greater and more long-lasting increase in intracellular $Ca^{2+}$. Otherwise, no difference in any other parameter related to fusion or fusion pore expansion was observed in cells stimulated by PACAP, DMPP, bethanechol, or carbachol. This suggests that the major differences in the actions of these agents are on steps upstream of the increase in $Ca^{2+}$.

### 4.2 | The physiological roles of PACAP and acetylcholine in the adrenal medulla

The notion that some other “non-cholinergic substance” released from splanchnic neurons may be responsible for maintaining tonic release of catecholamines during high rates of neural activity was first articulated by Wakade.[46] This was based on experiments showing catecholamine secretion rapidly desensitized when splanchnic input to the medulla was stimulated at high frequencies or when the medulla was continually perfused with acetylcholine. Remarkably, catecholamine release recovered if the stimulation frequency were suddenly decreased to 3 Hz from 10 Hz. The release stimulated by 3 Hz stimulation was insensitive to block by hexamethonium, a ganglionic blocking agent, and atropine, a classic muscarinic receptor antagonist. Catecholamine release stimulated at 3 Hz was even potentiated by phorbol esters. The known mechanisms by which PACAP operates makes it possible, if not likely, that it is this “non-cholinergic substance.”

Recently, arguments have been made that PACAP not only complements, but can even supplant acetylcholine as the dominant driver of chromaffin cell secretion. There is now convincing evidence that at higher rates of splanchnic activity, after nicotinic receptors are desensitized, PACAP can “take oved’ to sustain catecholamine release when the demand for secretion is high.[10,11] One of the major counterpoints to these arguments appears to be that, compared to acetylcholine, PACAP is a weaker secretagogue.[46,47] Our study does not address this issue directly. What it does provide is evidence that independently regulated pathways for secretion have evolved in the adrenal medulla. One presumes that such pathways, controlled as they are by different agonists, are very likely to serve physiological roles that are also not entirely overlapping.

The idea that peptides and small molecule neurotransmitters are released under different synaptic conditions has support in the literature (for an excellent review on this topic, see[48]). Peptide neurotransmitters may require higher stimulation frequencies for release. Other reports suggest that their release may depend on the precise pattern of activity.[49] While none of this helps us to “know” the conditions under which acetylcholine or PACAP are released from sympathetic nerve endings, it does suggest there are rules underpinning their release profiles. Going forward, it will be important to learn precisely what those rules are, and how this relates to the physiological function of the adrenal medulla.

## ACKNOWLEDGMENTS

Support was provided by NIH grants, R01GM106569 to CAA, R35GM127303 to AVS, R01NS122534 to AA, and the American Heart Association 17GRNT33661156 to KC.

## Funding information

American Heart Association, Grant/Award Number: 17GRNT33661156; National Institute of General Medical Sciences, Grant/Award Numbers: R01GM106569, R35GM127303; National Institute of Neurological Disorders and Stroke, Grant/Award Number: R01NS122534

## DATA AVAILABILITY STATEMENT

The data that support the findings of this study are available from the corresponding author upon reasonable request.

## REFERENCES

1. Goldstein DS. Adrenal responses to stress. Cell Mol Neurobiol. 2010;30(8):1433–1440. doi:10.1007/s10571-010-9606-9 [PubMed: 21061156]
2. Goldstein DS, Kopin IJ. Evolution of concepts of stress. Stress. 2007;10(2):109–120. doi:10.1080/10253890701288935 [PubMed: 17514579]
3. Cannon WB. The adrenal medulla. Bull N Y Acad Med. 1940;16(1):3–13. https://www.ncbi.nlm.nih.gov/pubmed/19312138 [PubMed: 19312138]
4. De Robertis E, Ferreira AV. Submicroscopic changes of the nerve endings in the adrenal medulla after stimulation of the splanchnic nerve. J Biophys Biochem Cytol. 1957;3(4):611–614. doi:10.1083/jcb.3.4.611 [PubMed: 13449104]
5. Grynszpan-Winograd O. Adrenaline and noradrenaline cells in the adrenal medulla of the hamster: a morphological study of their innervation. J Neurocytol. 1974;3(3):341–361. doi:10.1007/bf01097918 [PubMed: 4140222]
6. Feldberg W, Minz B, Tsudzimura H. The mechanism of the nervous discharge of adrenaline. J Physiol. 1934;81(3):286–304. doi:10.1113/jphysiol.1934.sp003136 [PubMed: 16994544]
7. Guerineau NC. Cholinergic and peptidergic neurotransmission in the adrenal medulla: a dynamic control of stimulus-secretion coupling. IUBMB Life. 2019;72:553–567. doi:10.1002/iub.2117 [PubMed: 31301221]
8. Carbone E, Borges R, Eiden LE, Garcia AG, Hernandez-Cruz A. Chromaffin cells of the adrenal medulla: physiology, pharmacology, and disease. Compr Physiol. 2019;9(4):1443–1502. doi:10.1002/cphy.c190003 [PubMed: 31688964]
9. Eiden LE, Emery AC, Zhang L, Smith CB. PACAP signaling in stress: insights from the chromaffin cell. Pflugers Arch. 2018;470(1):79–88. doi:10.1007/s00424-017-2062-3 [PubMed: 28965274]
10. Kuri BA, Chan SA, Smith CB. PACAP regulates immediate catecholamine release from adrenal chromaffin cells in an activity-dependent manner through a protein kinase C-dependent pathway. J Neurochem. 2009;110(4):1214–1225. doi:10.1111/j.1471-4159.2009.06206.x [PubMed: 19508428]
11. Stroth N, Kuri BA, Mustafa T, Chan SA, Smith CB, Eiden LE. PACAP controls adrenomedullary catecholamine secretion and expression of catecholamine biosynthetic enzymes at high splanchnic nerve firing rates characteristic of stress transduction in male mice. Endocrinology. 2013;154(1):330–339. doi:10.1210/en.2012-1829 [PubMed: 23221599]
12. Criado M. Acetylcholine nicotinic receptor subtypes in chromaffin cells. Pflugers Arch. 2018;470(1):13–20. doi:10.1007/s00424-017-2050-7 [PubMed: 28791474]
13. Zhou Z, Neher E. Calcium permeability of nicotinic acetylcholine receptor channels in bovine adrenal chromaffin cells. Pflugers Arch. 1993;425(5–6):511–517. http://www.ncbi.nlm.nih.gov/pubmed/7510879 [PubMed: 7510879]
14. Fenwick EM, Marty A, Neher E. Sodium and calcium channels in bovine chromaffin cells. J Physiol. 1982a;331:599–635. http://www.ncbi.nlm.nih.gov/pubmed/6296372 [PubMed: 6296372]
15. Garcia AG, Garcia-De-Diego AM, Gandia L, Borges R, Garcia-Sancho J. Calcium signaling and exocytosis in adrenal chromaffin cells. Physiol Rev. 2006;86(4):1093–1131. doi:10.1152/physrev.00039.2005 [PubMed: 17015485]

16. Inoue M, Matsuoka H, Harada K, Kao LS. Muscarinic receptors in adrenal chromaffin cells: physiological role and regulation of ion channels. Pflugers Arch. 2018;470(1):29–38. doi:10.1007/s00424-017-2047-2 [PubMed: 28762161]
17. Harada K, Matsuoka H, Miyata H, Matsui M, Inoue M. Identification of muscarinic receptor subtypes involved in catecholamine secretion in adrenal medullary chromaffin cells by genetic deletion. Br J Pharmacol. 2015;172(5):1348–1359. doi:10.1111/bph.13011 [PubMed: 25393049]
18. Fisher SK, Holz RW, Agranoff BW. Muscarinic receptors in chromaffin cell cultures mediate enhanced phospholipid labeling but not catecholamine secretion. J Neurochem. 1981;37:491–497. [PubMed: 7264672]
19. Olivos L, Artalejo AR. Muscarinic excitation-secretion coupling in chromaffin cells. Acta Physiol. 2008;192(2):213–220. doi:10.1111/j.1748-1716.2007.01816.x
20. Holman ME, Tonta MA, Coleman HA, Parkington HC. Muscarinic receptor activation in Guinea-pig chromaffin cells causes decreased membrane conductance and depolarization. J Auton Nerv Syst. 1998;68(3):140–144. doi:10.1016/s0165-1838(97)00122-7 [PubMed: 9626940]
21. Inoue M, Harada K, Matsuoka H, Nakamura J, Warashina A. Mechanisms and roles of muscarinic activation in Guinea-pig adrenal medullary cells. Am J Physiol Cell Physiol. 2012;303(6):C635–C644. doi:10.1152/ajpcell.00147.2012 [PubMed: 22744007]
22. Morales A, Mohan R, Chen X, et al. J Gen Physiol. 2023;155(2):1–22. doi:10.1085/jgp.202213180
23. Smith CB, Eiden LE. Is PACAP the major neurotransmitter for stress transduction at the adrenomedullary synapse? J Mol Neurosci. 2012;48(2):403–412. doi:10.1007/s12031-012-9749-x [PubMed: 22610912]
24. Hill J, Chan SA, Kuri B, Smith C. Pituitary adenylate cyclase-activating peptide (PACAP) recruits low voltage-activated T-type calcium influx under acute sympathetic stimulation in mouse adrenal chromaffin cells. J Biol Chem. 2011;286(49):42459–42469. doi:10.1074/jbc.M111.289389 [PubMed: 22009744]
25. Shigetomi E, Kracun S, Sofroniew MV, Khakh BS. A genetically targeted optical sensor to monitor calcium signals in astrocyte processes. Nat Neurosci. 2010;13(6):759–766. doi:10.1038/nn.2557 [PubMed: 20495558]
26. Gubernator NG, Zhang H, Staal RG, et al. Fluorescent false neurotransmitters visualize dopamine release from individual presynaptic terminals. Science. 2009;324(5933):1441–1444. doi:10.1126/science.1172278 [PubMed: 19423778]
27. Wightman RM, Jankowski JA, Kennedy RT, et al. Temporally resolved catecholamine spikes correspond to single vesicle release from individual chromaffin cells. Proc Natl Acad Sci U S A. 1991;88:10754–10758. [PubMed: 1961743]
28. Atchison DK, O'Connor CL, Menon R, et al. Hypertension induces glomerulosclerosis in phospholipase C-epsilon1 deficiency. Am J Physiol Renal Physiol. 2020;318(5):F1177–F1187. doi:10.1152/ajprenal.00541.2019 [PubMed: 32223311]
29. Wang H, Oestreich EA, Maekawa N, et al. Phospholipase C epsilon modulates beta-adrenergic receptor-dependent cardiac contraction and inhibits cardiac hypertrophy. Circ Res. 2005;97(12):1305–1313. doi:10.1161/01.RES.0000196578.15385.bb [PubMed: 16293787]
30. Bolte S, Cordeliers FP. A guided tour into subcellular colocalization analysis in light microscopy. Journal of Microscopy. 2006;224(3): 213–232. doi:10.1111/j.1365-2818.2006.01706.x [PubMed: 17210054]
31. Brindley RL, Bauer MB, Blakely RD, Currie KPM. An interplay between the serotonin transporter (SERT) and 5-HT receptors controls stimulus-secretion coupling in sympathoadrenal chromaffin cells. Neuropharmacology. 2016;110(Pt A):438–448. doi:10.1016/j.neuropharm.2016.08.015 [PubMed: 27544824]
32. Mosharov EV, Sulzer D. Analysis of exocytotic events recorded by amperometry. Nat Methods. 2005;2(9):651–658. doi:10.1038/nmeth782 [PubMed: 16118635]
33. Colliver TL, Hess EJ, Ewing AG. Amperometric analysis of exocytosis at chromaffin cells from genetically distinct mice. J Neurosci Methods. 2001;105(1):95–103. doi:10.1016/s0165-0270(00)00359-9 [PubMed: 11166370]

34. Dwivedi AK, Mallawaarachchi I, Alvarado LA. Analysis of small sample size studies using nonparametric bootstrap test with pooled resampling method. Stat Med. 2017;36(14):2187–2205. doi:10.1002/sim.7263 [PubMed: 28276584]
35. Akerboom J, Chen TW, Wardill TJ, et al. Optimization of a GCaMP calcium indicator for neural activity imaging. J Neurosci. 2012;32(40):13819–13840. doi:10.1523/JNEUROSCI.2601-12.2012 [PubMed: 23035093]
36. Chow RH, von Ruden L, Neher E. Delay in vesicle fusion revealed by electrochemical monitoring of single secretory events in adrenal chromaffin cells. Nature. 1992;356(6364):60–63. doi:10.1038/356060a0 [PubMed: 1538782]
37. Wightman RM, Schroeder TJ, Finnegan JM, Ciolkowski EL, Pihel K. Time course of release of catecholamines from individual vesicles during exocytosis at adrenal medullary cells. BiophysicalJ. 1995;68(1):383–390.
38. Chang CW, Chiang CW, Jackson MB. Fusion pores and their control of neurotransmitter and hormone release. J Gen Physiol. 2017;149(3):301–322. doi:10.1085/jgp.201611724 [PubMed: 28167663]
39. Zhou Z, Misler S, Chow RH. Rapid fluctuations in transmitter release from single vesicles in bovine adrenal chromaffin cells. Biophys J. 1996;70(3):1543–1552. doi:10.1016/S0006-3495(96)79718-7 [PubMed: 8785312]
40. Lewis MJ, Pelham HR. Ligand-induced redistribution of a human KDEL receptor from the Golgi complex to the endoplasmic reticulum. Cell. 1992;68(2):353–364. doi:10.1016/0092-8674(92)90476-s [PubMed: 1310258]
41. Oestreich EA, Malik S, Goonasekera SA, et al. Epac and phospholipase Cepsilon regulate Ca2+ release in the heart by activation of protein kinase Cepsilon and calcium-calmodulin kinase II. J Biol Chem. 2009;284(3):1514–1522. doi:10.1074/jbc.M806994200 [PubMed: 18957419]
42. Saternos HC, Almarghalani DA, Gibson HM, et al. Distribution and function of the muscarinic receptor subtypes in the cardiovascular system. Physiol Genomics. 2018;50(1):1–9. doi:10.1152/physiolgenomics.00062.2017 [PubMed: 29093194]
43. Ohta T, Wakade AR, Nakazato Y, Ito S. Ca(2+)-dependent K(+) current and exocytosis in responses to caffeine and muscarine in voltage-clamped Guinea-pig adrenal chromaffin cells. J Neurochem. 2001;78(6):1243–1255. doi:10.1046/j.1471-4159.2001.00502.x [PubMed: 11579133]
44. Dzhura I, Chepurny OG, Kelley GG, et al. Epac2-dependent mobilization of intracellular Ca(2)+ by glucagon-like peptide-1 receptor agonist exendin-4 is disrupted in beta-cells of phospholipase C-epsilon knockout mice. J Physiol. 2010;588(Pt 24):4871–4889. doi:10.1113/jphysiol.2010.198424 [PubMed: 21041529]
45. Nash CA, Brown LM, Malik S, Cheng X, Smrcka AV. Compartmentalized cyclic nucleotides have opposing effects on regulation of hypertrophic phospholipase Cepsilon signaling in cardiac myocytes. J Mol Cell Cardiol. 2018;121:51–59. doi:10.1016/j.yjmcc.2018.06.002 [PubMed: 29885334]
46. Wakade AR. Noncholinergic transmitter(s) maintains secretion of catecholamines from rat adrenal medulla for several hours of continuous stimulation of splanchnic neurons. J Neurochem. 1988;50(4):1302–1308. doi:10.1111/j.1471-4159.1988.tb10608.x [PubMed: 2894411]
47. Chowdhury PS, Guo X, Wakade TD, Przywara DA, Wakade AR. Exocytosis from a single rat chromaffin cell by cholinergic and peptidergic neurotransmitters. Neuroscience. 1994;59(1):1–5. doi:10.1016/0306-4522(94)90092-2 [PubMed: 7910672]
48. Cropper EC, Jing J, Vilim FS, Weiss KR. Peptide Cotransmitters as dynamic, intrinsic modulators of network activity. Front Neural Circuits. 2018;12:78. doi:10.3389/fncir.2018.00078 [PubMed: 30333732]
49. Verhage M, McMahon HT, Ghijsen WE, et al. Differential release of amino acids, neuropeptides, and catecholamines from isolated nerve terminals. Neuron. 1991;6(4):517–524. doi:10.1016/0896-6273(91)90054-4 [PubMed: 2015091]

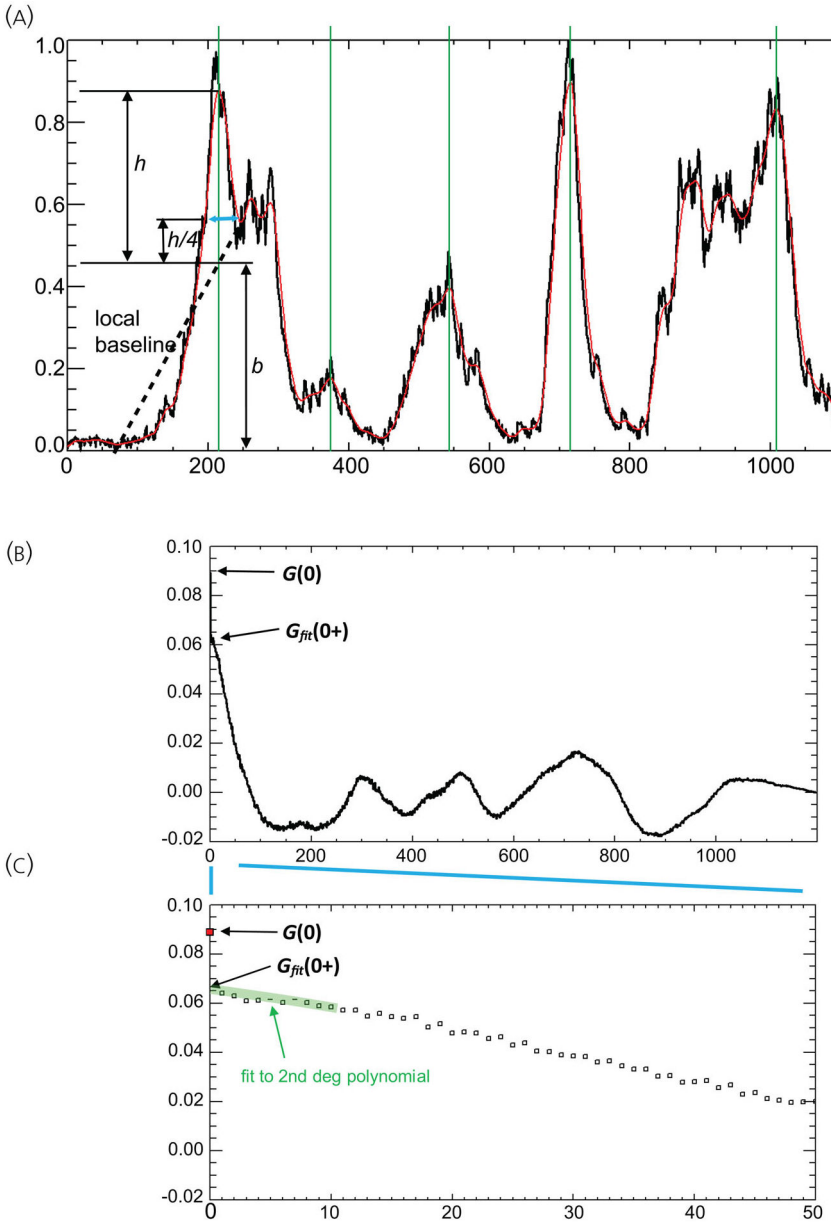


**FIGURE 1.**

Image analysis of $Ca^{2+}$ responses. (A) Measurement of spike height and width based on local baselines. Explanation of lines, colors, and variables is in the text. (B) Autocorrelation $G(L)$ of $\Delta F(t)$ vs. $t$. (C) The bottom panel is an expansion of the top to feature the smallest $L$. The data used here for illustrative purposes is the same unsmoothed curve that is shown in (A), but with one change: simulated (white) shot noise was added to the data to show the consequent appearance of a distinct discontinuous peak in the autocorrelation at $L = 0$ (shown here in red). The second degree polynomial fit to the first 10 points is shown in green.

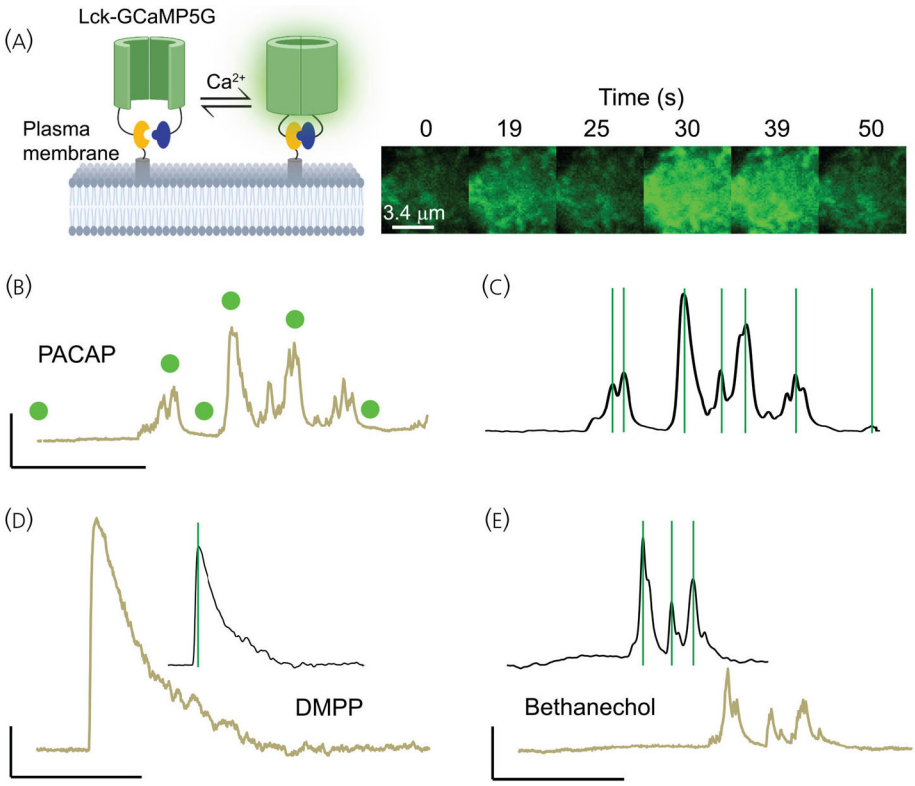


**FIGURE 2.**

Exemplar responses of mouse adrenal chromaffin cells expressing Lck-GCaMP5G to DMPP, bethanechol, and PACAP. (A) Cartoon depicting the Lck-GCaMP5G protein in the absence and presence of $Ca^{2+}$. The cartoon was created on BioRender and used here with permission. Right panel. Images of a cell expressing Lck-GCaMP5G prior to stimulation (time 0) and during stimulation with 1 µM PACAP. (B) %ΔF/F versus time record for the cell in (A). The green circles above the record correspond to times at which images in (A) were acquired. (C) Record in (A) was convolved with a Gaussian for smoothing. Green lines indicate fluorescent maxima detected by analysis algorithm. Many, but not all, maxima were automatically detected by the program. (D) Exemplar %ΔF/F versus time record for a cell stimulated by 1 µM DMPP. A smoothed curve with green line, indicating the position of a fluorescent maximum, is shown in inset. (E) Exemplar %ΔF/F versus time record for a cell stimulated by 100 nM bethanechol. Smoothed curve with green lines, indicating position of fluorescent maxima, is shown in inset. Scale for all records is: $x = 20$ s; $y = 20\%\Delta F/F$.

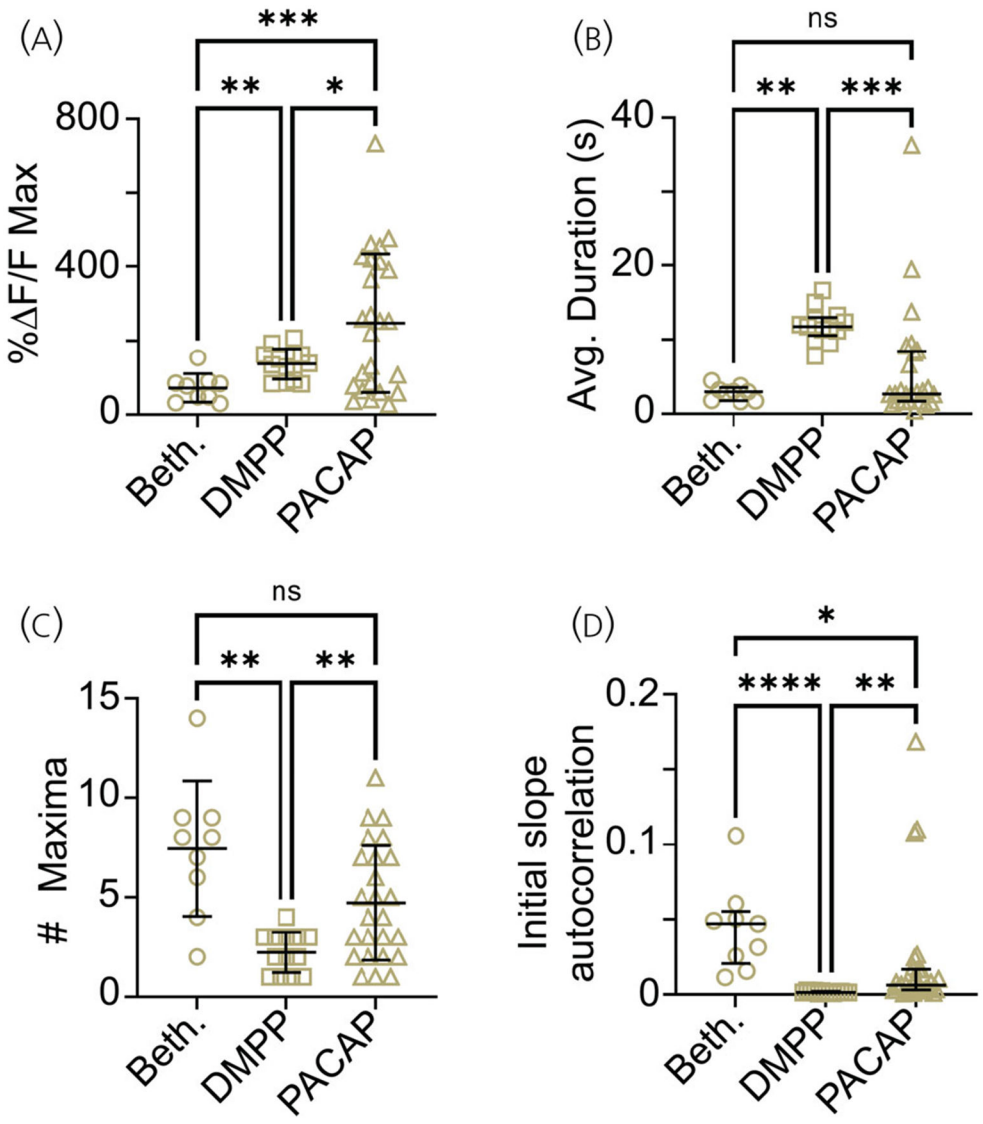


**FIGURE 3.**

Analysis of $Ca^{2+}$ responses triggered by DMPP, bethanechol, and PACAP. All statistical values are reported in Table 1; circle (bethanechol), square (DMPP), or triangle (PACAP). (A) The maximum amplitude measured in the record is indicated. Each symbol on the scatter plot represents a maximum value from a different record. The black line denotes mean, whiskers the standard deviation. (B) The time duration of the maximum is defined as its full width at height *h*/4 as measured up from its local baseline. Thus, the average duration represents the mean of the durations of all the acceptable maxima. The black line denotes means, whiskers the standard deviation. (C) Number of maxima detected that pass criterion test for maxima detection (described in Methods). The black line denotes median, whiskers the interquartile range. (D) Initial slope of the autocorrelation function values for DMPP are tightly clustered as the responses are highly regular with little variation. The values for PACAP, and especially bethanechol, exhibit a wide distribution; this reflects a “jitteriness”

in the ΔF/F records that is greater for PACAP and bethanechol than DMPP. The black line denotes mean, whiskers the interquartile range.

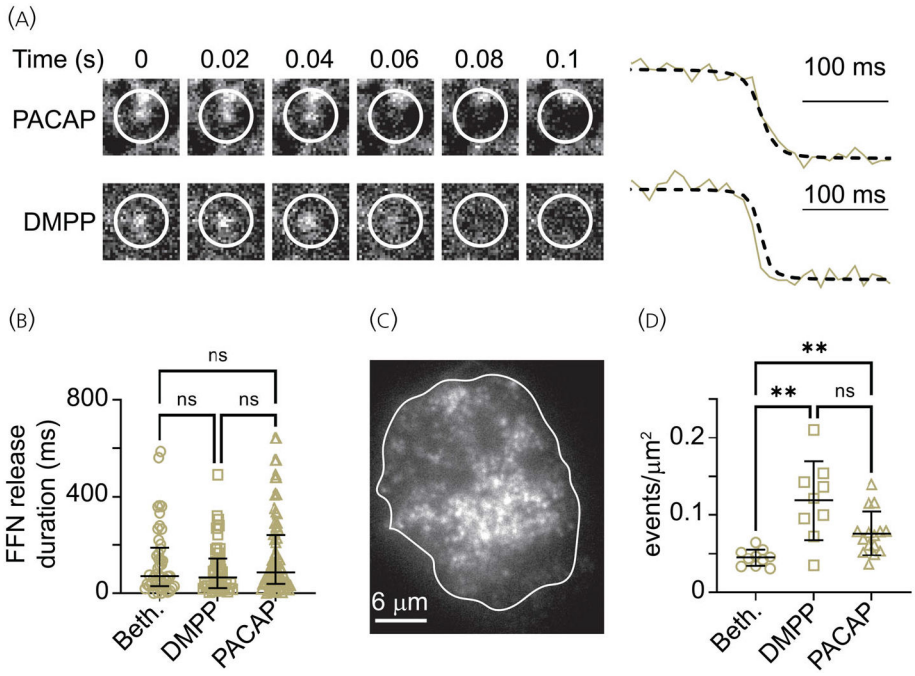


**FIGURE 4.**

Imaging of chromaffin cell secretory responses. (A) Two examples of fusion events, one stimulated by 1 µM PACAP, and the other, stimulated by 1 µM DMPP are shown. Time 0 is arbitrarily chosen as some time interval prior to fusion and release of FFN511. Circle diameter is approximately 1 µm. The corresponding intensity versus time records are on the right of the image series. A least-squares fitting procedure[22] is used to generate the fit indicated by the black dashed lines. (B) Time durations for the release of FFN511. Each symbol represents the release duration for single fusion event. *n*'s = 84, 48, 46 (PACAP, DMPP, bethanechol). Black line denotes median, whiskers the interquartile range (25th, 75th percentile): PACAP = 0.086 (0.038, 0.24); DMPP = 0.065 (0.021, 0.14); bethanechol = 0.070 (0.029,0.19). Kruskal-Wallis statistic 2.9, $p = .2$; bethanechol versus PACAP, $p > .99$; bethanechol versus DMPP, $p > 0.99$; DMPP versus PACAP, $p = .2$. (C) A chromaffin cell in which vesicles are loaded with FFN511. The footprint of the cell, used for measuring the surface area, is demarcated by a white line. (D) The number of fusion events/µm$^2$ of the cell footprint as a function of agonist stimulation. The black line denotes mean, whiskers the SD: PACAP = 0.076 ± 0.028, $n = 15$; DMPP = 0.12 ± 0.051, $n = 9$; bethanechol = 0.044 ± 0.011, $n = 10$. One-way ANOVA $F = 14.8$, $p = .0002$; bethanechol versus PACAP, $p = .003$; bethanechol versus DMPP, $p = .006$; DMPP versus PACAP, $p = .11$.

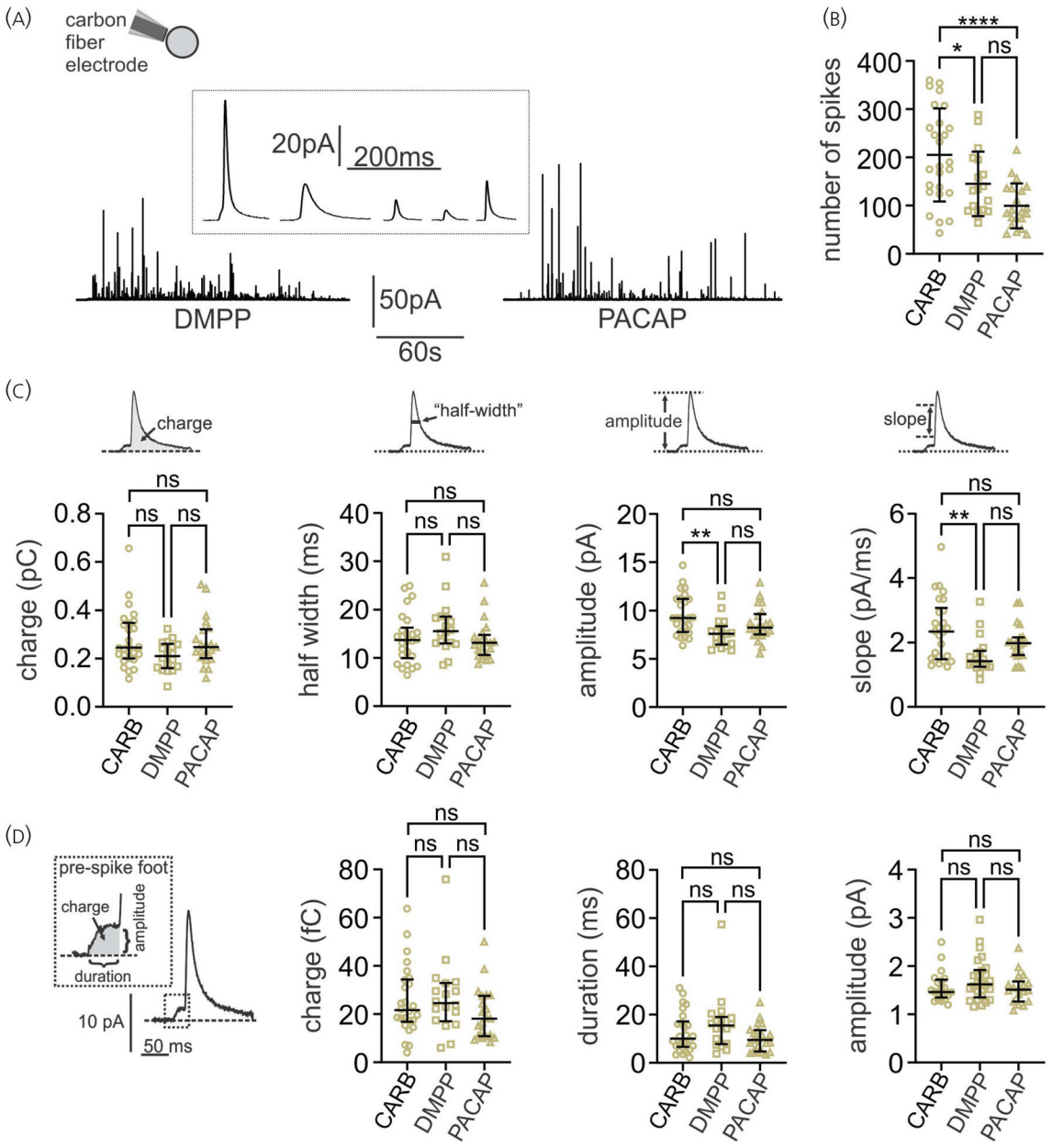


**FIGURE 5.**

The secretory response of mouse chromaffin cells detected with carbon fiber amperometry. (A) Secretion was evoked in mouse chromaffin cells using the non-selective cholinergic receptor agonist carbachol ($n = 26$), the nicotinic receptor agonist DMPP ($n = 18$) or PACAP ($n = 21$) and detected using carbon fiber amperometry. Representative traces are shown for cells stimulated with either DMPP or PACAP. The insert shows exemplary spikes from the cell stimulated with PACAP on an expanded scale. (B) The numbers of spikes (vesicle fusion events) evoked for each cell over a 3-min stimulation period are shown. Line denotes mean and whiskers the standard deviation. Statistical significance was determined using a one-way ANOVA ($F = 11.65$, $n < .001$) and Tukey's test for multiple pairwise comparisons as indicated on the graph (ns, not significantly different; *$p < .05$; ****$p$

< .0001). (C) All non-overlapping individual spikes were analyzed to determine average (median) values of spike charge, duration at half maximal amplitude (half-width), peak amplitude, and rising slope for each cell. Symbols represent individual cell values, line indicates the median, and whiskers the interquartile range (25th–75th percentile). Statistical significance was determined using a Kruskal-Wallis test followed by Dunn's test for multiple pairwise comparisons. There were no statistically significant differences between PACAP and either cholinergic agonist. The spike amplitude and slope were significantly smaller in cells stimulated with DMPP compared to carbachol (see Table 2 for a summary of spike parameters and statistical comparisons). (D) Some amperometric events display a prespike foot (see exemplary spike on left panel). There were no statistically significant differences in the median charge, duration, or amplitude of the pre-spike foot from cells stimulated with the different agonists (Kruskal-Wallis test; pairwise comparisons as indicated using Dunn's test) (see Table 3 for summary of spike parameters, foot parameters, and statistical comparisons).

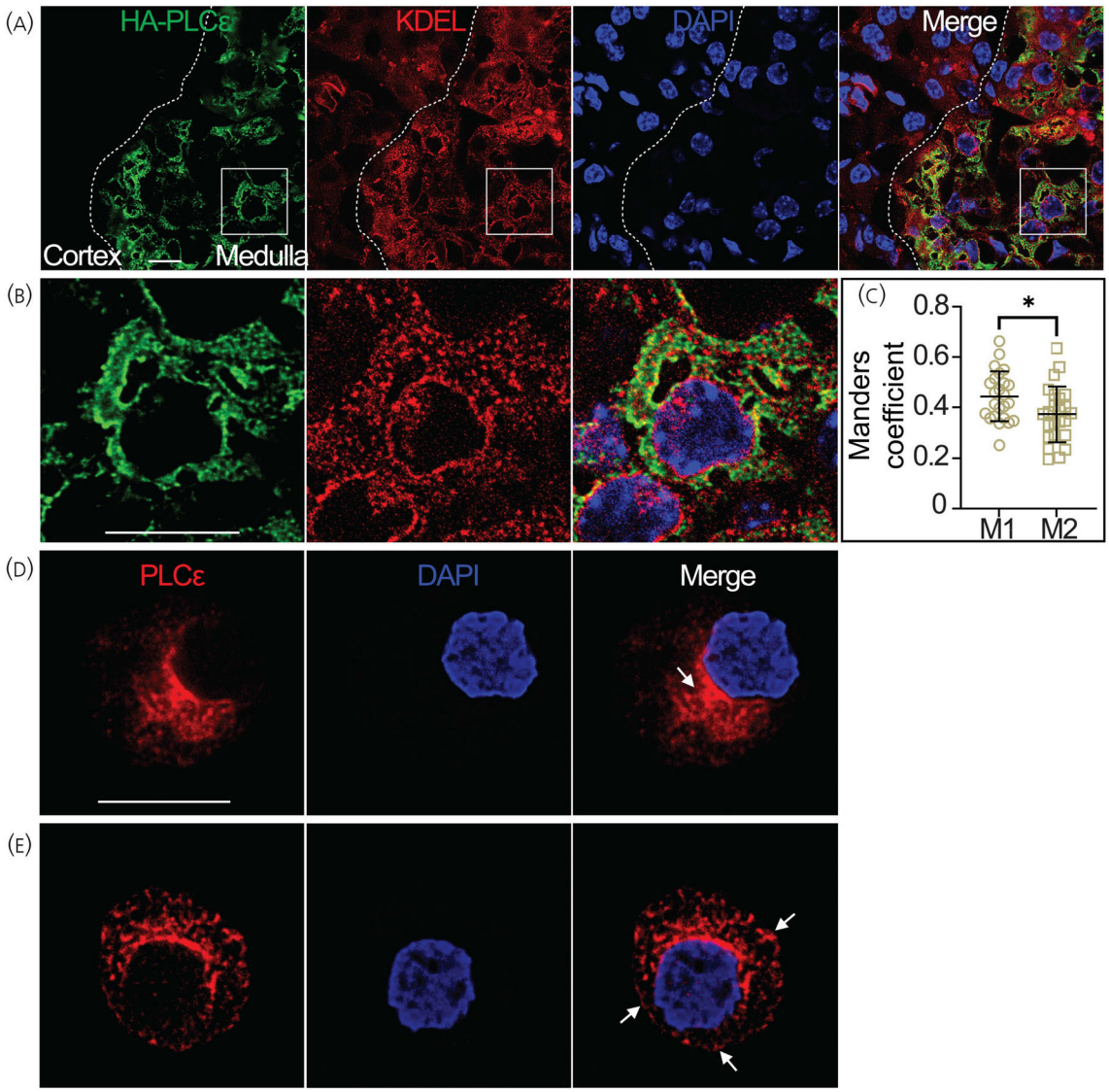


**FIGURE 6.**

Immunolocalization of PLCε in the mouse adrenal medulla. (A) Adrenal frozen sections taken from a HA-PLCε mouse labeled with DAPI, and with antibodies to HA and KDEL. (B) Region in square within (A) is expanded. (C) Manders colocalization coefficients were derived from JACoP ImageJ plugin. M1 represents the fraction of HA-PLCε colocalized with KDEL. M2 represents the fraction of KDEL colocalized with HA-PLCε. The black line denotes mean, whiskers the SD: M1 = 0.44 ± 0.10; M2 = 0.37 ± 0.11. Each symbol, circle or square, represents the Manders colocalization coefficient for one selected cell in the medulla. A total of 24 cells were used for analysis from 13 slices taken from five mice. Welch's *t*-test used for comparisons. M1 versus M2, $p = 0.02$. (D, E) Dissociated chromaffin cells labeled with an anti-PLCε antibody and with DAPI. Arrow in (D) represents a perinuclear region of the cell with abundant PLCε expression. Arrows in (E) indicate PLCε-labeling in what is likely the plasma membrane. Scale bars are 10 μm in all images.

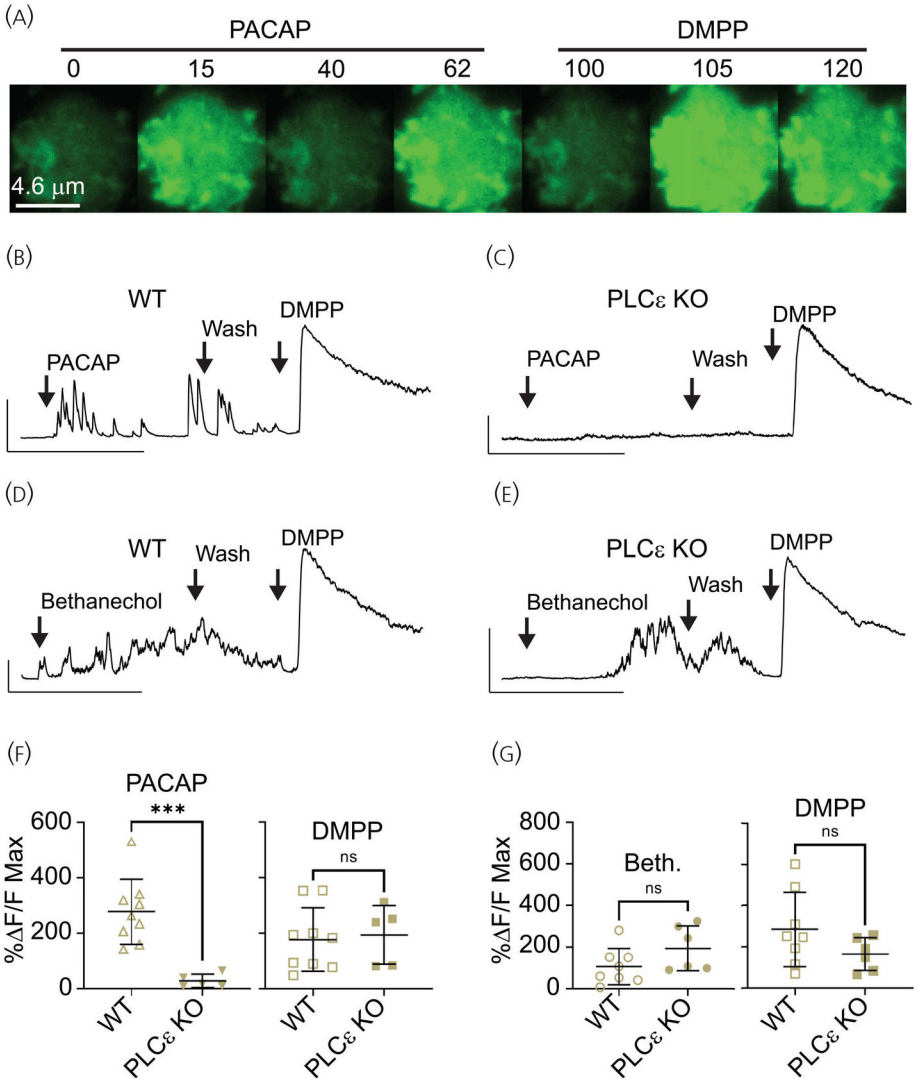


**FIGURE 7.**

$Ca^{2+}$ responses of WT and PLCɛ KO cells to DMPP, bethanechol, and PACAP. (A) A series of images showing an Lck-GCAMP5G-expressing WT chromaffin cell, sequentially stimulated with 1 µM PACAP and then 1 µM DMPP. Time after start of acquisition, in seconds, is indicated above each image. (B) Intracellular $Ca^{2+}$ levels fluctuate in response to PACAP. DMPP causes a sudden increase in $Ca^{2+}$ that reaches a peak and then monotonically decays. Arrows indicate periods when the PACAP, basal PSS wash, or DMPP were applied. (C) Agonists were applied in the same sequence to PLCɛ KO cells. Little to no response to PACAP was observed. (D) WT chromaffin cells were stimulated with 100 nM bethanechol, then a basal PSS wash, and then DMPP. (E) PLCɛ KO cells were stimulated with bethanechol and then DMPP. (F) Means ± SD for PACAP %ΔF/F max: WT cells, 280 ± 120, $n = 9$; KO cells, 27 ± 24, $n = 5$. Means ± SD for DMPP %ΔF/F max: WT cells, 180 ± 110, $n = 9$; KO cells, 190 ± 110. Welch's $t$-test comparisons: PACAP WT versus KO, $p = .0002$; DMPP WT versus KO, $p = .8$. (G) Means ± SD for bethanechol %ΔF/F max: WT cells, 110 ± 31, $n = 8$; KO cells, 190 ± 110, $n = 6$. Means ± SD for DMPP %ΔF/F max: WT

cells, 280 ± 64, $n = 8$; KO cells, 160 ± 32, $n = 6$. Welch's $t$-test comparisons: Bethanechol WT versus KO, $p = .1$; DMPP WT versus KO, $p = .1$. Scale for all records in Figure 7: $x = 50$ s, $y = 100\%\Delta F/F$. In all graphs, the black line denotes means, whiskers the standard deviation.

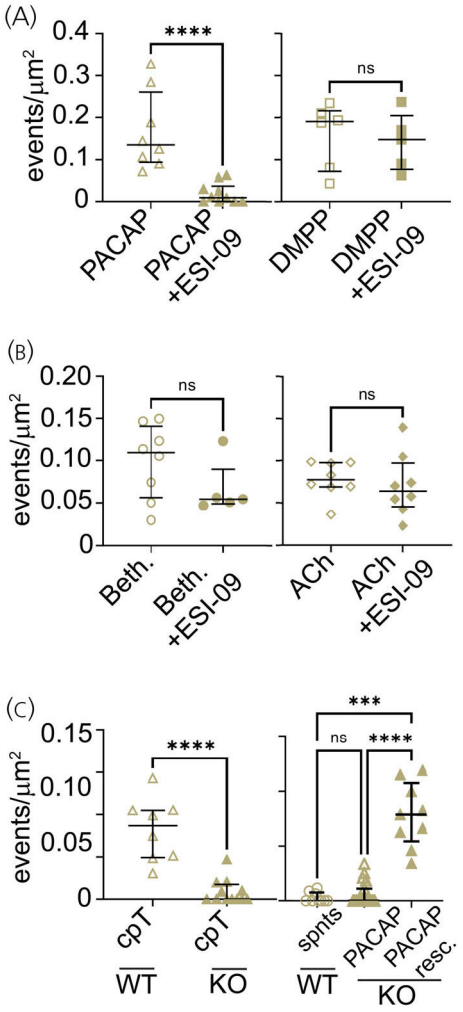


**FIGURE 8.**

Secretory responses of WT and PLCε KO cells in the presence of select agonists and antagonists. (A, B) PACAP-evoked secretion is blunted when 1 μM ESI-09 is included in the extracellular solution. However, secretory responses to 100 μM ACh, 100 nM bethanechol (beth.), and 1 μM DMPP were not disrupted by ESI-09. Black line denotes median, whiskers the interquartile range. Median (25th, 75th) values are as follows: PACAP, 0.14 (0.094,0.27), $n = 8$; PACAP + ESI-09, 0.0092 (0,0.037), $n = 10$; DMPP, 0.19 (0.071, 0.22), $n = 6$; DMPP + ESI-09,0.15 (0.077, 0.20), $n = 5$; beth., 0.11 (0.056, 0.14), $n = 8$; beth. +ESI-09, 0.055 (0.049, 0.090), $n = 5$; ACh, 0.078 (0.069, 0.099), $n = 8$; ACh + ESI-09, 0.064 (0.045, 0.097), $n = 8$. Mann–Whitney comparisons: PACAP versus PACAP+ESI-09, $p = .00005$; Beth. versus Beth. +ESI-09, $p = .3$. Welch's $t$ test comparisons: DMPP versus DMPP + ESI-09, $p = .7$; ACh versus ACh + ESI-09, $p = .6$. (C) (left) The secretory response to cpTOME (cpT) is disrupted in PLCε KO cells. Black line denotes median, whiskers the interquartile range. Median (25th, 75th) values are as follows: cpT in WT, 0.087 (0.049, 0.11), $n = 8$; cpT in KO, 0 (0, 0.017), $n = 12$. Mann–Whitney, $p = .00003$. (right) PACAP-stimulated release in KO cells is not different that spontaneous (“spnts”) release in WT cells. PACAP-stimulated release in KO cells is rescued when PLCε is overexpressed (“PACAP resc.”). Black line

denotes median, whiskers the interquartile range. Median (25th, 75th) values are as follows: spnts, 0 (0, 0.0075), $n = 9$; PACAP in KO, 0 (0, 0.011), $n = 19$; PACAP rescue, 0.79 (0.054, 0.11), $n = 9$. Kruskal-Wallis statistic 23, $p = 7.4 \times 10^{-6}$. PACAP (KO) versus spnts (WT), $p > .99$; PACAP (WT) versus PACAP rescue, $p = .00001$; spnts (WT) versus PACAP rescue, $p = .0002$.

**TABLE 1**

Summary of $Ca^{2+}$ signal properties.

| Parameter | Bethanechol (*n* = 9 cells) | DMPP (*n* = 13 cells) | PACAP (*n* = 29 cells) | Statistical comparison |
|---|---|---|---|---|
| %ΔF/F Max | 72 (SD 38) | 140 (SD 41) | 248 (SD 188) | One-way ANOVA $F = 13$, $p = .00009$ |
| Average duration of maxima (s) | 3.0 (1.8, 3.5) | 12 (11, 13) | 2.7 (1.7, 8.4) | Kruskal-Wallis statistic 16, $p = .0003$ |
| # maxima | 7.4 (SD 3.4) | 2.2 (SD 1.0) | 4.7 (SD 2.9) | One-way ANOVA $F = 18$, $p = .00007$ |
| Initial slope of the autocorrelation | 0.047 (0.021 0.055) | 0.0015 (0.0013, 0.0021) | 0.006 (0.0031, 0.017) | Kruskal-Wallis statistic 25, $p = 3 \times 10^{-7}$ |

*Note*: Data are reported as mean with standard deviation (SD) and compared using one-way ANOVA with Tukey's test for multiple pairwise comparisons; alternatively, data are reported as median with interquartile range (25th, 75th percentile) and compared using Kruskal-Wallis (non-parametric one-way ANOVA) with Dunn's test for multiple pairwise comparisons. Pairwise comparisons as follows: %ΔF/F Max: bethanechol versus PACAP, $p = .0004$; bethanechol versus DMPP, $p = .004$; DMPP versus PACAP, $p = .09$. Avg. duration: bethanechol versus PACAP, $p > .99$; bethanechol versus DMPP, $p = .002$; DMPP versus PACAP, $p = .0002$. # Maxima: bethanechol versus PACAP, $p = .1$; bethanechol versus DMPP, $p = .004$; DMPP versus PACAP, $p = .001$. Initial slope of the autocorrelation: bethanechol versus PACAP, $p = .03$; bethanechol versus DMPP, $p = 1 \times 10^{-6}$; DMPP versus PACAP, $p = .001$.

## TABLE 2

Summary of amperometric spike parameters.

| Parameter | Carbachol (*n* = 26 cells) | DMPP (*n* = 18 cells) | PACAP (*n* = 21 cells) | Statistical comparison |
|---|---|---|---|---|
| Total number of spikes per cell | 205 (SD 96) | 145 (SD 67) | 99 (SD 46) | One-way ANOVA $F = 12$, $p < .0001$ |
| Number of non-overlapping spikes per cell | 106 (SD 48) | 94 (SD 42) | 61 (SD 21) | One-way ANOVA $F = 7.7$, $p < .01$ |
| Spike charge (pC) | 0.25 (0.2, 0.35) | 0.21 (0.16, 0.26) | 0.25 (0.2, 0.32) | Kruskal-Wallis statistic 4.4, $p = .11$ |
| Spike amplitude (pA) | 9.2 (7.8, 11) | 7.6 (6.5, 8.4) | 8.2 (7.5, 9.7) | Kruskal-Wallis statistic 11, $p = .004$ |
| Spike half width (ms) | 14 (9.9, 16) | 16 (13, 19) | 13 (11, 15) | Kruskal-Wallis statistic 3.7, $p = .16$ |
| Spike slope (pA/ms) | 2.3 (1.5, 3.1) | 1.4 (1.2, 1.7) | 2.0 (1.6, 2.2) | Kruskal-Wallis statistic 11, $p = .005$ |

*Note*: Numbers of spikes are reported as mean with standard deviation (SD) and compared using one-way ANOVA with Tukey's test for multiple pairwise comparisons. Individual spike parameters (charge, amplitude, half-width, slope) were determined only for non-overlapping events, reported as median with interquartile range (25th, 75th percentile), and compared using Kruskal-Wallis test (non-parametric one-way ANOVA) with Dunn's test for multiple pairwise comparisons. Pairwise comparisons for parameters with statistically significant differences are as follows: Total number of spikes: Carbachol versus PACAP, $p < .0001$; Carbachol versus DMPP, $p = .03$; DMPP versus PACAP, $p = .15$. Number of non-overlapping spikes: Carbachol versus PACAP, $p < .0008$; Carbachol versus DMPP, $p = .59$; DMPP versus PACAP, $p = .032$. Spike amplitude: Carbachol versus PACAP, $p = .35$; Carbachol versus DMPP, $p = .0026$; DMPP versusPACAP, $p = .239$. Spike slope: Carbachol versus PACAP, $p = .95$; Carbachol versus DMPP, $p = .0035$; DMPP versus PACAP, $p = .087$.

## TABLE 3

Summary of amperometric events with a prespike foot.

| | **Carbachol (*n* = 26 cells)** | **DMPP (*n* = 18 cells)** | **PACAP (*n* = 21 cells)** | **Statistical comparison** |
|---|---|---|---|---|
| Number of spikes with a foot per cell | 19 (SD 11) | 10 (SD 6) | 11 (SD 7) | One-way ANOVA $F = 6.9$, $p < .01$ |
| Percent of spikes with foot | 18 (SD 8) | 11 (SD 5) | 17 (SD 6) | One-way ANOVA $F = 5.3$, $p < .01$ |
| Spike charge (pC) | 0.49 (0.41, 0.64) | 0.51 (0.39, 0.7) | 0.5 (0.36, 0.61) | Kruskal-Wallis statistic 0.47, $p = .79$ |
| Spike amplitude (pA) | 34 (21, 49) | 29 (14, 42) | 27 (21, 46) | Kruskal-Wallis statistic 1.1, $p = .58$ |
| Spike half width (ms) | 8.8 (6.3, 14.1) | 11 (8.4, 14) | 7.6 (5.5, 14) | Kruskal-Wallis statistic 3.3, $p = .19$ |
| Spike slope (pA/ms) | 11 (5.8, 22) | 7.8 (2.8, 16) | 9.1 (5.4, 23) | Kruskal-Wallis statistic 1.7, $p = .44$ |
| Foot charge (fC) | 22 (17, 34) | 25 (17, 33) | 18 (11, 28) | Kruskal-Wallis statistic 3.4, $p = .18$ |
| Foot duration (ms) | 10 (6.7, 17) | 16 (7.8, 19) | 9.5 (4.7, 14) | Kruskal-Wallis statistic 3.9, $p = .14$ |
| Foot amplitude (pA) | 1.6 (1.4, 1.9) | 1.5 (1.3, 1.7) | 1.5 (1.3, 1.7) | Kruskal-Wallis statistic 2.2, $p = .33$ |

*Note*: Data is from the same groups of cells as Table 2 but parameters were calculated only from non-overlapping events that displayed a prespike foot. Spike number and percent of spikes with a foot are reported as mean with standard deviation and compared using one-way ANOVA with Tukey's test for multiple pairwise comparisons. Spike and foot parameter data are reported as median with interquartile range (25th, 75th percentile values). Statistical comparison was performed using a Kruskal-Wallis test (non-parametric one-way ANOVA) with Dunn's test for multiple pairwise comparisons. The percent of spikes preceded by a foot was significantly smaller in cells stimulated with DMPP compared to both carbachol and PACAP. Pairwise comparisons as follows: Percent of spikes with foot: Carbachol versus PACAP, $p = .9$; Carbachol versus DMPP, $p = .008$; DMPP versus PACAP, $p = .034$. However, there were no statistically significant differences in overall spike (charge, amplitude, half-width, slope), or prespike foot parameters (foot charge, foot duration, foot amplitude).